minerals

MDPI

Article

Gemstones from the Medicean Collection of the Natural History Museum of Florence (Italy): New Insights from Micro-Raman and PIXE-PIGE Analyses

Lucilla Fabrizi [1,2,*], Massimo Chiari [3,4], Vanni Moggi Cecchi [2], Rosarosa Manca [1] and Marco Benvenuti [1,5]

[1] Earth Sciences Department, University of Florence, 50121 Firenze, Italy; rosarosa.manca@unifi.it (R.M.); m.benvenuti@unifi.it (M.B.)
[2] Museo "La Specola"-University Museums System, University of Florence, 50125 Firenze, Italy; vanni.moggicecchi@unifi.it
[3] National Institute of Nuclear Physics, Division of Florence, 50019 Sesto Fiorentino, Italy; chiari@fi.infn.it
[4] Department of Physics and Astronomy, University of Florence, 50019 Sesto Fiorentino, Italy
[5] Institute of Geosciences and Georesources, National Research Council, 56124 Pisa, Italy
* Correspondence: lucilla.fabrizi@unifi.it

Abstract: The initial nucleus of gemstones at the Natural History Museum of the University of Florence (Italy) is linked to the significant collection of the Medici family, who began it as early as the 15th century. The present research aims to study this collection in order to (1) comprehensively review the archival and catalogue information available; (2) identify the mineralogical species correctly; and (3) gather information on the potential provenance of the gem deposits. To address these objectives, fifty gems were investigated using entirely non-invasive methods, ensuring the preservation of the collection's precious and historical value. All specimens underwent autoptic observation and micro-Raman analysis, while a selection was further examined using PIXE-PIGE to characterise their chemical composition, including trace elements. The gems were attributed to seven mineral species: emerald, topaz, grossular, cordierite, quartz, orthoclase, and tourmaline. One gem was identified as a fake, made of glass and likely produced in the 17th century. Twenty-nine of the historical attributions in the catalogue were found to be incorrect and were subsequently revised. In some cases, the trace elements and mineral inclusions identified in the gems enabled the determination of potential provenance deposits, which were then compared with the available archival information.

Keywords: ancient gemstones; emerald; topaz; grossular; cordierite; trace element concentration; museum collection; ion beam analysis; Raman microscopy

Academic Editor: Adrián Durán Benito

Received: 16 December 2024
Revised: 15 January 2025
Accepted: 17 January 2025
Published: 21 January 2025

Citation: Fabrizi, L.; Chiari, M.; Moggi Cecchi, V.; Manca, R.; Benvenuti, M. Gemstones from the Medicean Collection of the Natural History Museum of Florence (Italy): New Insights from Micro-Raman and PIXE-PIGE Analyses. *Minerals* **2025**, *15*, 96. https://doi.org/10.3390/min15020096

1. Introduction

The origins of gemstone collection are lost throughout the centuries. Kings, grand duchies, and princes loved to possess magnificent gems to display as symbols of wealth and power. The members of the House of Medici, who ruled over Florence, Italy, from the 15th until the 18th century, must have shared the same sentiment; indeed, small pieces of glyptic art seem to play a prominent role among the first artefacts they collected. The first to begin the family collection was Cosimo di Giovanni de' Medici (1389–1464) and the earliest documents referring to it date back to his son Piero the Gouty (1416–1469) who initiated the formation of an impressive family collection. Successors like Lorenzo the Magnificent (1449–1492) continued this endeavour with passion and interest. The collection included a remarkable variety of engraved gems, cameos, and hardstone objects, some of which

were very famous, e.g., the Farnese Cup [1]. Between 1574 and 1587, Francesco I de' Medici (1541–1587) decided to gather the family collection at the Uffizi Gallery in Florence [2]. In 1737, the House of Habsburg-Lorraine succeeded the House of Medici on the throne of the Grand Duchy of Tuscany.

With the foundation of the "Imperial and Royal Museum of Physics and Natural History" in 1775 by the Habsburg-Lorraine Grand Duke Peter Leopold in the Palazzo Torrigiani [3], part of the Medici collection, including several of the pieces now belonging to the "Collection of Carved Stones", was relocated there. However, as in the case of collections of similar families, intricate political events led to the partial dispersal of the collection over the centuries. Nowadays some artefacts of the collection are in different institutions, among them the National Archaeological Museum in Naples and the British Museum in London [4].

Between the 19th and 20th centuries, the collections of the Peter Leopold Museum were redistributed across various museum sites in Florence, only to be reunited under a single administrative framework in 1984 as part of the Museum of Natural History. Since 2018, they have been included in the Museum System of the University of Florence [5,6]. As said above, the Mineralogical and Lithological Collection, which includes the Medicean gemstones, is presently housed in the Museo La Specola, located in the Palazzo Torrigiani, the former site of Peter Leopold's museum.

Despite the availability of numerous written sources, documents, and historical catalogues accompanying the mineralogical artefacts of the Medici's gemstone collection, detailed information on individual specimens remains significantly fragmented. When a museum collection has a complex acquisition history and has been relocated multiple times, it is often challenging to confidently link specific pieces to their catalogue descriptions. This difficulty is compounded when the objects lack sufficiently diagnostic or distinctive features, as is often the case with gemstones. Moreover, identifying mineral species can be particularly challenging in objects that no longer exhibit their natural crystal habits, having undergone cutting and polishing. This is especially true for gemstones catalogued in the past, when specialised instruments for mineralogical identification were either unavailable or not easily accessible. For all these reasons, the most recent catalogue available at the museum, dating back to 1943/1947, may contain incomplete or imprecise information on ancient gemstones and therefore requires thorough verification and revision. In the present paper, any mention of the collection's catalogue will refer to the one dated 1943/1947, despite the existence of older catalogues and documents that are not explicitly relevant to the purpose of this work.

The first results of a scientific study on the oldest core of the gemstone collection of Museo La Specola are presented in the present paper. This project aimed to verify (and, if necessary, correct) the mineralogical classification of the specimens and, where possible, compare them with data from original documents and catalogues concerning the provenance and formation environments of the gemstones, based on their chemical (e.g., trace elements) and mineralogical characteristics. This information is also extremely valuable for the conservation of artefacts of great value.

Due to the significance of the selected gemstones, only non-destructive and non-invasive analytical methods were employed for this study, namely micro-Raman spectroscopy and ion beam analysis (IBA), particularly particle-induced X-ray emission (PIXE) and proton-induced gamma-ray emission (PIGE), both of which are widely used on a broad range of museum objects. Micro-Raman is widely adopted for the rapid and precise identification of various types of mineral-based artefacts [7], e.g., mineral specimens [8], gemstones [9], reliquaries [10], and jewellery with gemstones [11,12]. On the other hand, the combined and simultaneous use of PIXE and PIGE techniques has provided interesting

results in studies on cultural heritage samples for the wide range of chemical elements they can quantitatively detect (including light elements that are challenging to analyse with other techniques) in a completely non-invasive and non-deliberately destructive manner [13–16]. These methods have been used to study gemstones such as emeralds [17–19], garnets [20–23], and various others [24,25], providing valuable insights into their potential provenance and genetic processes.

2. Materials and Methods

The investigated materials were a selection of the earliest gemstones of the museum collection, which already appear in the 1793 catalogue, the earliest available catalogue of the collection, potentially dating back to the Medici period. A total of twenty-three inventory entries were identified, which describe the fifty gemstones analysed (Figure 1), since in some cases, a series of specimens were catalogued under the same inventory number. Table 1 reports the museum numbers currently in use and the provenance for each sample, as recorded in the 1943/1947 catalogue, along with additional information on weight and cut. When multiple gemstones are listed under a single catalogue number, they are distinguished with a letter. In the catalogue attributions, the samples were classified under seven different mineral species: beryl, garnet, orthoclase, quartz, spinel, and topaz. No sample retains its natural habit; all have undergone cutting and/or polishing processes, some of which exhibit very ancient features.

Table 1. List of the gems analysed in this study, including their mineralogical identification. n.a. = not available.

Sample n.		Weight (g)	Processing	Provenance (From Label)	Identification (From Label)	Mineralogical Identification (This Study)	Inclusions
13158		31.0	Octagon mixed cut	n.a.	Quartz	Quartz	
13161		4.0	Pear cut	n.a.	Rutilated quartz	Rutilated quartz	Rutile
13165		3.1	Simple oval cabochon	n.a.	Rutilated quartz	Quartz	Hematite
13172		23.8	Antique square cut	n.a.	Hyaline quartz	Quartz	
13177		2.2	Antique mixed octagon cut	Brazil	Quartz	Quartz	Hematite
13182		30.2	Mixed octagon cut	n.a.	Quartz	Quartz	
13199		4.6	Mixed octagon cut	n.a.	Quartz	Quartz	
13207	a	0.7	Oval cabochon	n.a.	Amethyst quartz	Cordierite	
	b	0.2	Rectangular step cut	n.a.	Amethyst quartz	Quartz	
	c	0.3	Antique, mixed, octagon cut	n.a.	Amethyst quartz	Amethyst quartz	
	d	0.4	Antique, elongated, octagon cut	n.a.	Amethyst quartz	Cordierite	
	e	0.4	Oval cabochon	n.a.	Amethyst quartz	Cordierite	
	f	0.6	Drilled, smoothed and polished	n.a.	Amethyst quartz	Cordierite	
	g	4.2	Drilled, rose oval cut	n.a.	Amethyst quartz	Cordierite	
	h	0.3	Rose cut with concave pavillon	n.a.	Amethyst quartz	Cordierite	
	i	0.6	Oval cabochon with concave pavillon	n.a.	Amethyst quartz	Cordierite	
	j	0.5	Pear cabochon with concave pavillon	n.a.	Amethyst quartz	Cordierite	

Table 1. *Cont.*

Sample n.		Weight (g)	Processing	Provenance (From Label)	Identification (From Label)	Mineralogical Identification (This Study)	Inclusions
	k	0.8	Oval cabochon with concave pavillon	n.a.	Amethyst quartz	Cordierite	
	l	0.7	Drilled, smoothed and polished	n.a.	Amethyst quartz	Cordierite	
	m	0.6	Drilled, smoothed and polished	n.a.	Amethyst quartz	Cordierite	
	n	0.4	Antique, mixed octagon cut	n.a.	Amethyst quartz	Amethyst Quartz	
	o	0.9	Rectangular step cut	n.a.	Amethyst quartz	Amethyst Quartz	
13333		1.1	Oval cabochon	East Indies	Carnelian quartz	Quartz	
13355	a	0.5	Modified cabochon	n.a.	Onyx	Quartz	
	b	0.9	Cabochon	n.a.	Onyx	Quartz	
13394		2.4	Oval cabochon	n.a.	Agathe quartz	Quartz	Hematite
13403		0.4	Flattened, simple cabochon	Zweibrücken Duchy, Germany	Agathe quartz	Quartz	Iron oxides
13539	a	3.0	Oval cabochon	Saxony, Germany	Topaz	Topaz	
	b	0.4	Oval cabochon	Saxony, Germany	Topaz	Quartz	
13541	a	0.8	Rectangular step cut	Saxony, Germany	Topaz	Quartz	
	b	0.6	Rectangular	Saxony, Germany	Topaz	Quartz	
13550		1.5	Rose cut with concave pavilion	n.a.	Almandine garnet	Glass	
13561	a	2.1	Heart-shaped rose cut	n.a.	Zircon	Grossular	Apatite
	b	3.2	Drilled rose cut	n.a.	Zircon	Grossular	
	c	4.5	Ancient octagonal cut	n.a.	Zircon	Grossular	
	d	2.8	Ancient octagonal cut	n.a.	Zircon	Grossular	
13562	a	5.1	Rose cut with octagonal shape	n.a.	Zircon	Grossular	Apatite
	b	3.2	Ancient octagonal cut	n.a.	Zircon	Grossular	
	c	4.1	Ancient cut squared and polished	n.a.	Zircon	Grossular	
	d	3.2	Ancient cut squared and polished	n.a.	Zircon	Grossular	Apatite
	e	2.3	Ancient cut squared and polished	n.a.	Zircon	Grossular	
13587	a	7.2	Polished—broken specimen	Brazil	Beryl var emerald	Beryl (var. emerald)	
	b	2.3	Polished—broken specimen	Brazil	Beryl var emerald	Beryl (var. emerald)	
13601	a	1.0	Squared and polished	Brazil	Beryl var emerald	Beryl (var. emerald)	
	b	1.9	Squared and polished	Brazil	Beryl var emerald	Beryl (var. emerald)	
	c	0.4	Cabochon	Brazil	Beryl var emerald	Quartz	
13624		0.2	Table cut with rectangular shape	n.a.	Beryl var aquamarine	Topaz	
13677		2.8	Double cabochon	European Russia	Orthoclase	Quartz	
13678		0.4	Double cabochon with flattened, oval shape	Switzerland	Orthoclase	Orthoclase	
13706		21.0	Polished (similar to tumbled cut)	Sri Lanka	Spinel	Tourmaline	

Figure 1. The fifty analysed gemstones. Images property of the Museum of Natural History, University Museum System, Litho-Mineralogical Collection, University of Florence.

Two instruments were used for the micro-Raman analyses. Most samples were analysed with an Horiba Jobin-Yvon LabRam-IR Raman spectrometer, equipped with a HeNe laser source (λ = 632.8 nm) and an Olympus PX41 optical microscope. The detector was a silicon CCD cooled with a Peltier effect sensor at approximately −70 °C. The LabSpec

5 software managed the instrumentation, as well as the acquisition and processing of analytical data. This equipment was provided by the Museum System and the MEMA service centre of the University of Florence, Florence (Italy). The other instrument used was a Renishaw RM 2000, which uses an Ar+ ion laser source (λ = 514.5 nm) and a diode laser source (λ = 785 nm). It was equipped with a Leica DLML optical microscope with 5×, 20×, and 50× objectives, as well as a 60× long-working-distance objective. The detector was a RenCam CCD, electrically cooled to −70 °C. The instrument was operated with GRAMS/32 software at the Department of Chemistry "Ugo Schiff" of the University of Florence, Florence (Italy). Collection times were between 30 and 100 s, with three accumulations.

PIXE and PIGE analyses were conducted at the INFN LABEC laboratory in Florence (Italy) [26], which houses a 3 MV Tandetron accelerator equipped with a beamline specifically designed for low-current, non-destructive measurements on cultural heritage samples in an external beam setup [27]. A proton beam with an initial energy of 3.00 MeV was extracted into the atmosphere through a 200 nm thick Si_3N_4 membrane, and samples were positioned at 8 mm from the extraction window. After accounting for energy loss in the Si_3N_4 window and the atmospheric path, the proton energy at the sample surface was evaluated to be 2.95 MeV. The beam spot was defined by a circular collimator, 0.5 mm in diameter, placed in vacuum before the extraction window, while beam scanning over the surface sample was managed using micrometric stepper motors, enabling continuous scanning over a 5–10 mm line to minimise the impact of potential local inhomogeneities.

The beam current, indirectly measured using a rotating chopper [28], was maintained at a few hundred pA to ensure that the dead time remained below a few percent. Each measurement lasted 300 s. The experimental setup for PIXE-PIGE measurements included two X-ray detectors for PIXE: a small-area Silicon Drift Detector (SDD) with a 10 mm^2 active area (collimated to 3.5 mm^2) and a helium flow to reduce low-energy X-ray absorption for light element analysis (Na-Ca) and a large-area SDD with a 150 mm^2 active area and a 450 μm Mylar absorber for mid-heavy and trace elements (>Ca). Additionally, a High-Purity Germanium (HPGe) gamma-ray detector with 20% relative efficiency and a mechanical cooler was used for PIGE measurements.

PIXE spectra were processed using GUPIXWIN software, version 3.0.3 [29], analysing elements starting from Na. Instrumental parameters for quantitative analysis were calibrated using X-ray spectra from external reference materials, such as NIST 1412 and BCR 126A (for the small- and large-area SDDs) and NIST 610 (for the large-area SDD exclusively).

PIGE was employed to determine Be, F, and Na concentrations using nuclear reactions $^{9}Be(p,\alpha'\gamma^{1-0})^{6}Li$, $^{19}F(p,p'\gamma^{1-0})^{19}F$, and $^{23}Na(p,p'\gamma^{1-0})^{23}Na$, which produce gamma rays with energies of 3562 keV, 197 keV, and 441 keV, respectively. The gamma-ray peaks of interest in the PIGE spectra were fitted with gaussian functions to obtain peak areas. Quantitative analysis of Be and Na was then carried out through a comparison of the gamma-ray yield with those obtained from the measurements of thick BeO and NIST 1412 and BCR 126A glass standards, respectively. Lacking a certified external standard for fluorine, for the quantitative analysis of F, PIGRECO software, version 1.0 [30] was applied for a standardless interpretation of the PIGE data, integrating details of the experimental setup and measured differential cross-sections for proton-induced gamma-ray emission from F [31]. Detection limits are reported in Table S1 of the Supplementary Materials. Table S2 of the Supplementary Materials presents the chemical compositions of the samples, including major, minor, and trace elements for each analysed specimen. The sources of the estimated uncertainties reported in Table S2 are peak fitting and spectral deconvolution as statistical contributions and a calibration procedure with external standards as a systematical contribution.

3. Results and Discussion

After the autoptic observation of all the pieces, it was necessary to proceed with an analytical verification of their mineralogical attribution, as well as, where possible, of their provenance or geological origin. Several entries in the catalogues appeared, in fact, to be likely incorrect. All pieces were subjected to micro-Raman analysis for mineralogical identification. Some gems, either individually or as part of a series of objects with similar characteristics, underwent PIXE-PIGE analysis to obtain a more in-depth characterisation through the analysis of major, minor, and trace elements. The following species were analysed by PIXE-PIGE: emerald (four crystals), topaz (two, one blue and the other yellow), garnet (nine), cordierite (eleven), quartz (three), and one synthetic sample. The following sections discuss the results for each mineralogical species identified by this study.

3.1. Beryl var. Emerald

Five gemstones were classified as emeralds from Brazil in the catalogue. Emerald is the green variety of beryl ($Be_3Al_2Si_6O_{18}$), a cyclosilicate containing Cr, V, and Fe, which impart the intense green colour to the mineral. Its crystal structure is formed by hexagonal rings of silica tetrahedra connected to each other by Be tetrahedra and Al octahedra. The channels formed by the rings can host impurities (e.g., Fe^{2+}, Mg^{2+}, Mn^{2+}, or Li^{+}) [32].

Among these specimens, only four samples were confirmed as beryls by micro-Raman analyses (Figure 2a). PIXE-PIGE spectra (Figure 2b) validate the identification as emerald showing the presence of Cr, V, and Fe. The Raman identification is based on the main band at 1069 cm^{-1}, attributed to the Be-O bond, the bands at 325, 389, 623, and 686 cm^{-1}, associated with the ring vibrations [32,33], and the band at 1012 cm^{-1}, corresponding to the Si-O bond stretching [32,34]. These bands are typically observed in spectra from natural emeralds. The spectra in this study do not show bands related to specific deposits [32]. However, the band at 1298 cm^{-1}, present in samples 13587b and 13601a, is not commonly found in emeralds from Brazil according to Moroz et al. [32]. Nevertheless, it is difficult to determine the origin of a specimen solely based on these results.

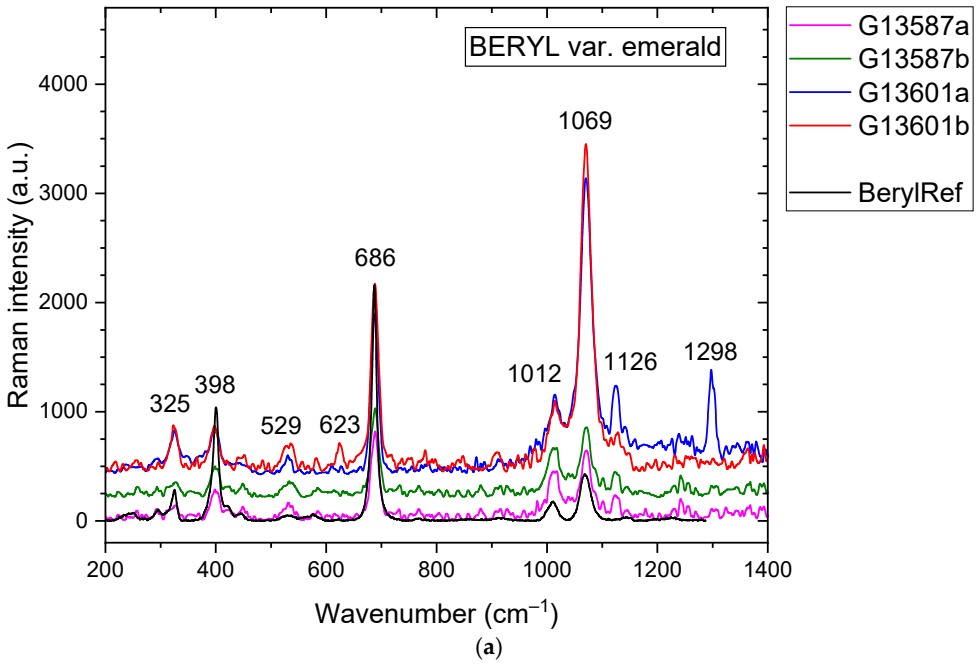

(**a**)

Figure 2. *Cont.*

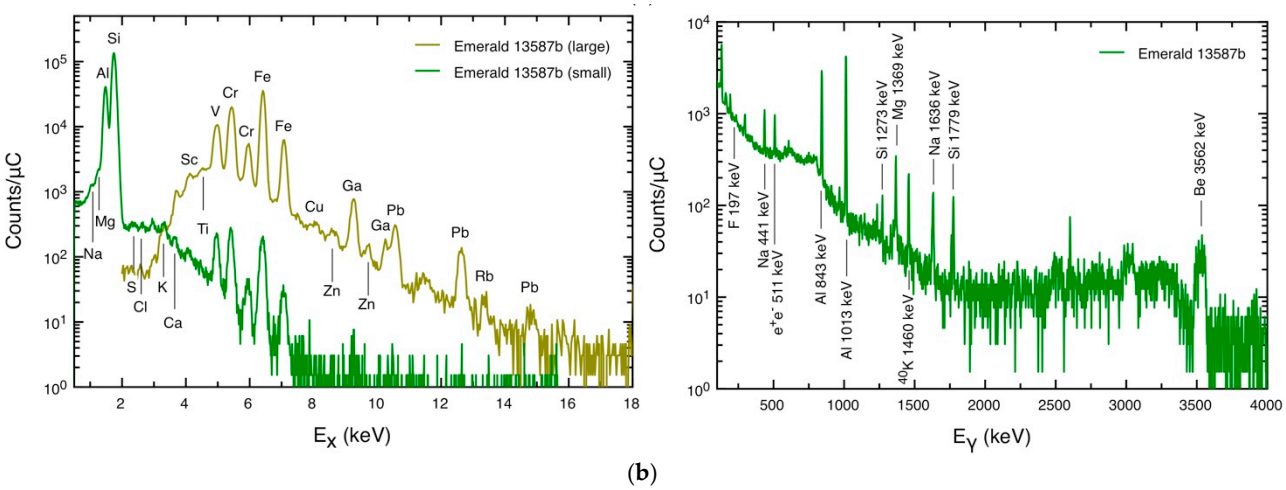

(**b**)

Figure 2. (**a**) Raman spectra from the gems identified as beryl, confirmed as emerald by PIXE-PIGE analyses. The spectrum used as reference (black line) is n. R050065 from the RRUFF database [35,36]. (**b**) PIXE spectra obtained with the two detectors (**left**) and PIGE spectrum (**right**), all normalised to the collected beam charge, from a gem identified as beryl var. emerald.

There are over fifty recognised emerald deposits around the world, and many studies address the issue of characterising a single deposit or identifying chemical parameters useful for distinguishing different deposits distributed globally [37–45]. According to Giuliani et al. [46], there are two types of deposits: Tectonic–Metamorphic-related, found in metamorphic and sedimentary environments, and Tectonic–Magmatic-related, found in granitic environment.

Although the analysis of trace elements remains the most powerful method for the discrimination of emerald provenance [19,40,42,45], some insights can also be gained by considering the composition of major elements. In this study, emeralds (Table S2 in Supplementary Materials) show medium–high Al_2O_3 content (16.8–17.6 wt%) and low Na_2O (0.3–0.6 wt%) and MgO (0.4–0.8 wt%) content compared to emeralds of different provenances analysed using destructive techniques [42,46]. This condition is usually associated with deposits that are related neither to granites nor to pegmatites [32,46].

The trace element patterns of emeralds show significant differences related to their original geological environment; in particular, emeralds associated with sedimentary environments are quite different from those associated with igneous and metamorphic rocks [45].

A selection of trace elements (Li, Cs, Sc, V, Cr, Ga, Fe, and Rb) determined in our samples were compared with those of the most important emerald deposits gathered by Alonso-Perez et al. [45]. These multi-incompatible trace elements have been demonstrated to be the most statistically significant for discriminating deposits [45,47]. It is important to highlight that although our samples have been part of the collection since a date prior to 1793, it was decided to not exclude data from deposits that the literature indicates as recently discovered. This is because past trade routes for these kinds of objects are often unknown and, in some cases, may lead to unexpected results regarding the undocumented exploitation of deposits that were officially discovered at later dates. Figure 3a shows the patterns of the emeralds analysed in this study alongside the most compatible patterns of the average deposit samples from the work of Alonso-Perez et al. [45]: Colombia and Afghanistan. Brazil is included because it is indicated as the place of origin on the historical labels, but it does not show a high compatibility with the studied emeralds. Colombia and Afghanistan are both metamorphic-related emeralds deposits and can share a similar chemical signature with low concentrations of alkalis and Fe, but Colombian emeralds often

exhibit the highest chemical purity [45,47]. The binary plots in Figure 3b (four samples from this study compared with data from [45]) seam to reinforce the attribution to Colombian deposits and to rule out Afghanistan as a likely source. In fact, the samples from this study show lower concentrations of Sc and V compared to Afghan deposits and overlap with the range characteristic of Colombian deposits. Moreover, the four samples in this study show low concentrations of Fe content (284–569 ppm) and Rb (from b.l.d to 3.5 ppm) (Table S2), significantly lower than the average values reported for Brazilian deposits (average content of Fe = 5120 ppm and Rb = 31.4 ppm [47]) and Afghan deposits (average content of Fe = 3784 ppm and Rb = 46.9 ppm [47]). However, a partial ambiguity regarding the attribution to either deposit remains and further investigation using other spectroscopic techniques (e.g., FTIR) and/or inclusions analysis could be decisive in determining a definitive attribution to one of the two deposits.

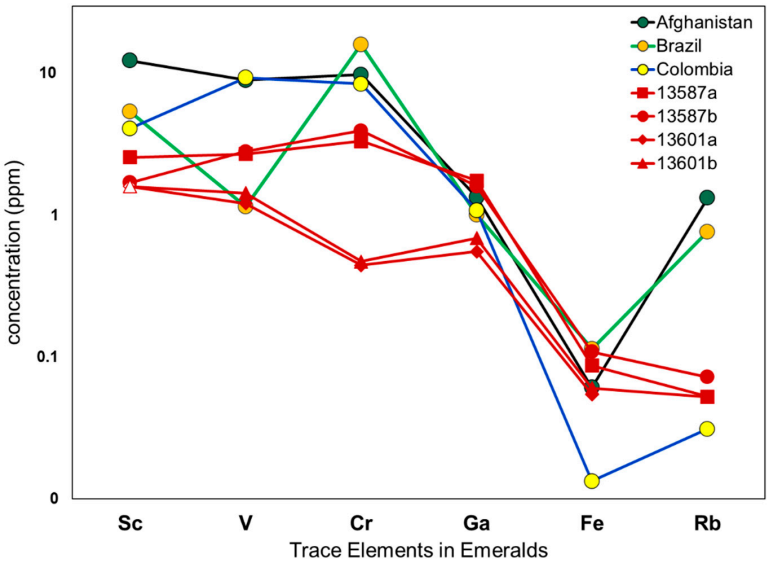

(**a**)

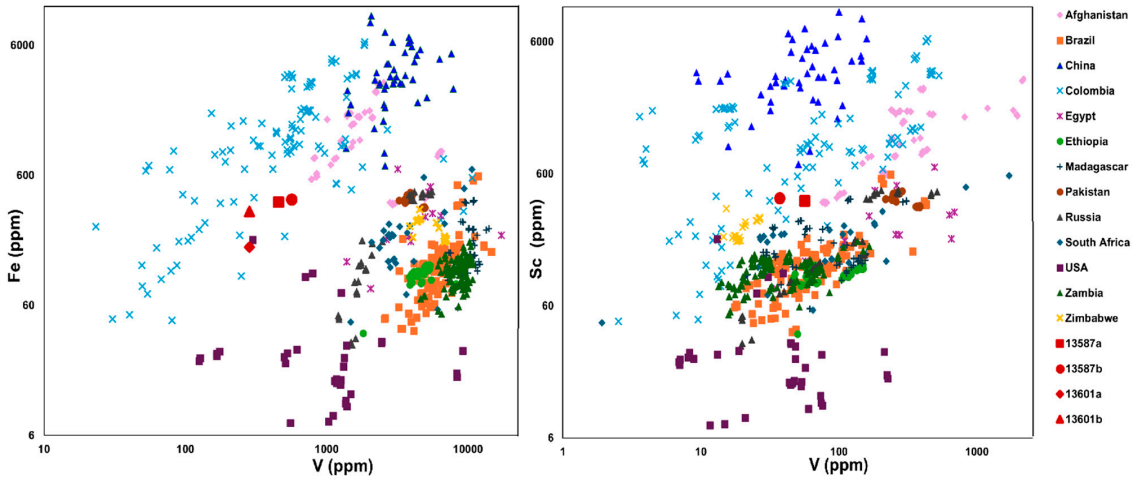

(**b**)

Figure 3. (**a**) Average composition of multi-incompatible trace elements (all the data are normalised to the bulk composition of the continental crust (CC) from Rudnick and Gao [48] of emerald from this study compared to the most compatible deposits, i.e., Afghanistan and Colombia, and Brazil from Alonso-Perez et al. [45]. (**b**) Binary plots of V versus Fe (**left**) and Sc (**right**) concentrations of emeralds from different deposits (data from Alonso-Perez et al. [45]) and the emeralds studied in this paper.

It can be concluded that, among the four identified emeralds (i.e., 13587a, 13587b, 13601a, 13601b), the attribution of their provenance to Brazil is likely incorrect. Their chemical signatures show greater compatibility with Colombian deposits, which possess unique and distinctly different geochemical and structural characteristics compared to those of Brazil.

3.2. Topaz

Topaz is a nesosilicate with the formula $Al_2SiO_4(F,OH)_2$. Hydroxyl groups are present, substituting for fluorine atoms, and the OH/(OH + F) ratio is the major variation in the chemical formula of the species, varying between almost zero and 30% [49]. The crystal structure is organised with groups of SiO_4 tetrahedra linked to octahedra chains of $Al[O_4(F,OH)_2]$ [50,51].

According to the 1943/1947 catalogue, specimens 13539a, 13539b, 13541a, and 13541b should be topaz, but the analyses confirmed this attribution only for 13539a; moreover, the analyses also identified 13624 as a blue topaz, and not as a beryl var. aquamarine (Table 1), as suggested by the earlier compilers of the catalogue, who were probably misled by the bluish colour of the gemstone.

The identification as topaz was preliminarily carried out through micro-Raman investigations (Figure 4a), based on the main band at 919 cm^{-1}, associated with Si-O stretching, secondary bands associated with other Si-O vibration modes (335 cm^{-1}) or the translation of the SiO_4 tetrahedra (244, 264, 274, 294 cm^{-1}), and the band at 1156 cm^{-1} attributed to the Al-OH bond [51,52].

Topaz occurs in several deposits in each continent associated with different kinds of lithotypes: magmatic rocks (felsic, pegmatites, and also post-magmatic), hydrothermal veins, and high-temperature, high-pressure metamorphic rocks [53–55]. Many studies have focused on the petrological, geochemical, and mineralogical characterisation of individual deposits of different natures [56–63], whereas fewer studies have compared multiple deposits with the aim of identifying distinctive fingerprints for them and reporting sufficiently detailed geochemical data [55,64–66]. The abundance of existing topaz deposits, the lack of a reference database, and the variability in trace element composition in topaz [53] make it challenging to attribute a single gemstone to a specific deposit. This difficulty is also highlighted in other studies [55,64], which have noted significant overlaps when attempting to experimentally discriminate the provenance of topaz samples using geochemistry and trace element concentrations. Nevertheless, some considerations can be drawn from both the fluorine and trace element content measured in our samples (Figure 4b).

Sample 13624 shows a fluorine content 16.5 wt%, while in the yellow sample 13539a, the fluorine content is 12.8 wt% (Table S2). Soufi [67] demonstrated that the F content can lead to several considerations about the formation environment of topaz but is not a parameter that can be used to discriminate between different deposits. The concentration of F in sample 13624 is common in several types of deposits, both magmatic and hydrothermal. Among the magmatic ones, pegmatites, topaz-bearing granites, and rhyolites can be excluded because they lead to the formation of fluorine-rich topaz (usually exceeding 17 wt%). Topazites and transitional magmatic hydrothermal systems can be excluded for the same reason. On the contrary, hydrothermal deposits related to post-magmatic metasomatic processes (e.g., greisens, quartz veins, etc.) usually contain topaz with F content between 10.7 wt% and 16.0 wt% F and are thus compatible with our samples [67].

Localities that primarily supplied topaz to Europe in historical time include Germany and the Czech Republic [53,68], and sample 13539a is said to originate from Saxony in the catalogue; however, only sample 13624 has F content compatible with these areas. For instance, the hydrothermal formation of greisens hosted in the Vykmanov granite stock in

the Czech Republic contains topaz with F content ranging from 15.16 to 16.78 wt%, while the hydrothermal greisens from the Triberg granite complex in southwest Germany contain topaz with approximately 16.20 wt% of F. With higher F concentrations, the magmatic Eibenstock granite, located on the border between Germany and the Czech Republic, can also be considered, as its topaz has F content ranging from 16.09 to 21.00 wt% [67], or the hydrothermal breccia-pipe deposit at Schneckenstein, in the Erzgebirge region (Saxony, Germany), although topaz with this origin seems more F-enriched (~17.43 wt%) [68] than sample 13624. In addition to this, it is known that many topaz gemstones commercialised in Europe originate from Brazil, particularly from the famous hydrothermal Ouro Preto mine (Minas Gerais, Brazil) [53], which is renowned for its magnificent imperial topaz. This deposit contains topaz with F content ranging from 11.66 to 17.66 wt% [67]. Both our samples fall within this range.

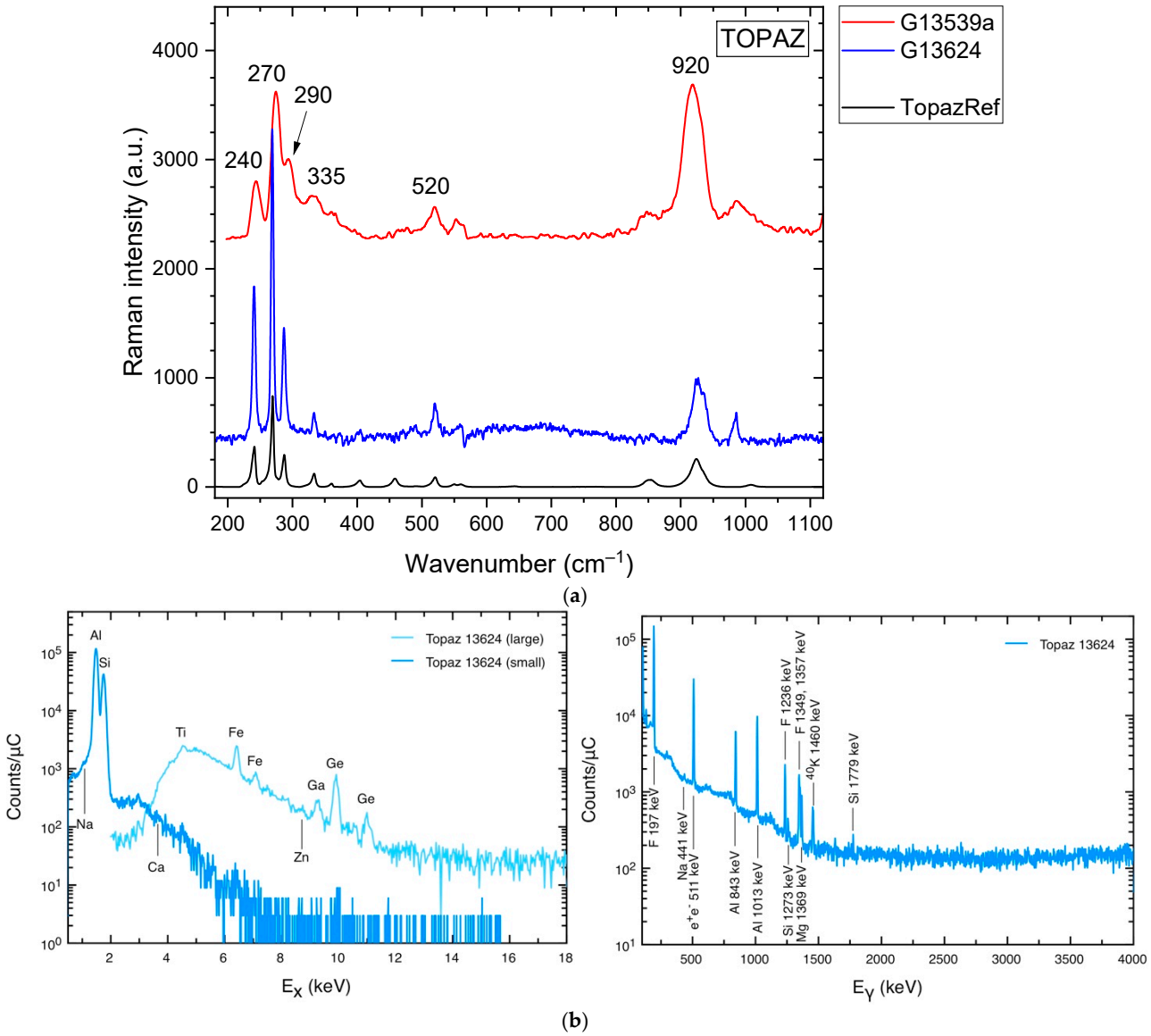

Figure 4. (**a**) Raman spectra from the gems identified as topaz. The spectrum used as a reference (black line) is n. R050404 from the RRUFF database [36]. (**b**) PIXE spectra obtained with the two detectors (**left**) and PIGE spectrum (**right**), all normalised to the collected beam charge from a gem identified as topaz.

The trace element compositions of the two topazes in this study show different patterns (Figure 5). Both samples are characterised by low amounts of Ge and Ga, which supports the hydrothermal origin of these gemstones [65]. Sample 13539a shows the presence of P, V, Cr, Mn, Cu, As, and Pb, which are not revealed in sample 13624. The Fe and Zn contents are higher in 13539a compared to sample 13624. The presence of P in the topaz correlates with the P content of the rocks in the deposits [65]. The high content of V, Cr, Mn, Fe, Cu, and Zn is likely correlated with the interaction of the crystallising fluid with BIF iron bodies [55]. This, along with the range of concentrations of Ti, Cr, V, Cu, Zn, Fe, Ge, and Ga revealed, is compatible with topaz from the Ouro Preto mine in Brazil [63].

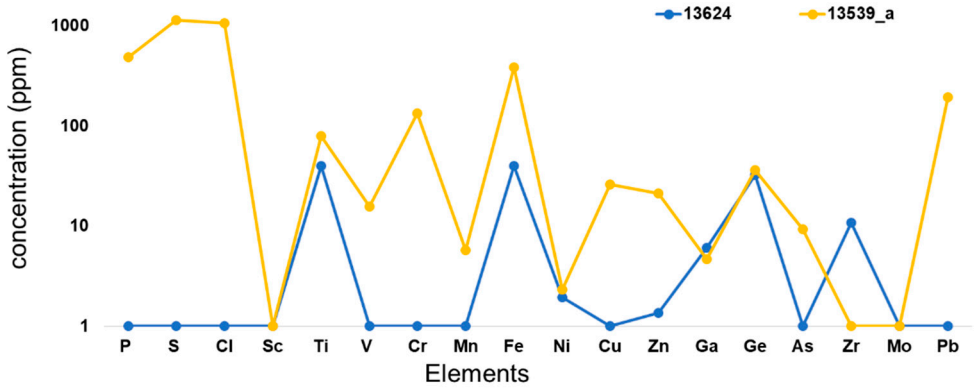

Figure 5. Trace elements patterns of the two topaz gemstones analysed in this study.

In conclusion, it is not possible to determine a definite provenance for the analysed specimens, but it appears that the two topazes formed in a hydrothermal environment in two different deposits and that sample 13539a is compatible with the Brazilian mineralization of imperial topaz, particularly considering the gem's warm and intense yellow colour. Conversely, the European origin of the topaz in this study is not supported by the acquired data.

3.3. Grossular

Grossular is a member of the garnet group of minerals. This is a group of nesosilicates with a general chemical formula $X_3Y_2(SiO_4)_3$, where X represents the divalent cations Ca^{2+}, Mg^{2+}, Fe^{2+}, or Mn^{2+}, and Y represents the trivalent cations Al^{3+}, Fe^{3+}, or Cr^{3+}. The garnet group presents two solid solution series. The pyralspite series with the general formula $[Mg,Fe,Mn]_3Al_2(SiO_4)_3$, where the end members are pyrope (Mg), almandine (Fe), and spessartine (Mn), and the ugrandite series with general formula $Ca_3[Cr,Al,Fe]_2(SiO_4)_3$ and uvarovite (Cr), grossular (Al), and andradite (Fe) as end members [69].

In the catalogue, only sample 13550 was defined as a garnet, whereas the other nine specimens (13561a,b,c,d and 13562a,b,c,d,e) were recognised as garnet in this study.

The identification as grossular was carried out by micro-Raman. The main band at 880 cm^{-1} corresponds to the stretching of the Si-O bond (Figure 6a). Additional bands associated with this vibration are observed at 827 cm^{-1} and 1007 cm^{-1} [70,71]. Bands at 417 cm^{-1} and 549 cm^{-1} are attributed to O–Si–O bending modes, while those at 179 cm^{-1} and 375 cm^{-1} correspond to the movement of SiO_4 tetrahedra [70,71]. Finally, the translations of divalent cations are responsible for the bands at 247 cm^{-1} and 278 cm^{-1} [70,71]. Moreover, Raman analysis allowed us to identify apatite inclusions in samples 13561a, 13562a, and 13562d (main bands at 965, 432, 581, and 592 cm^{-1}, as shown in Figure 6b) [33].

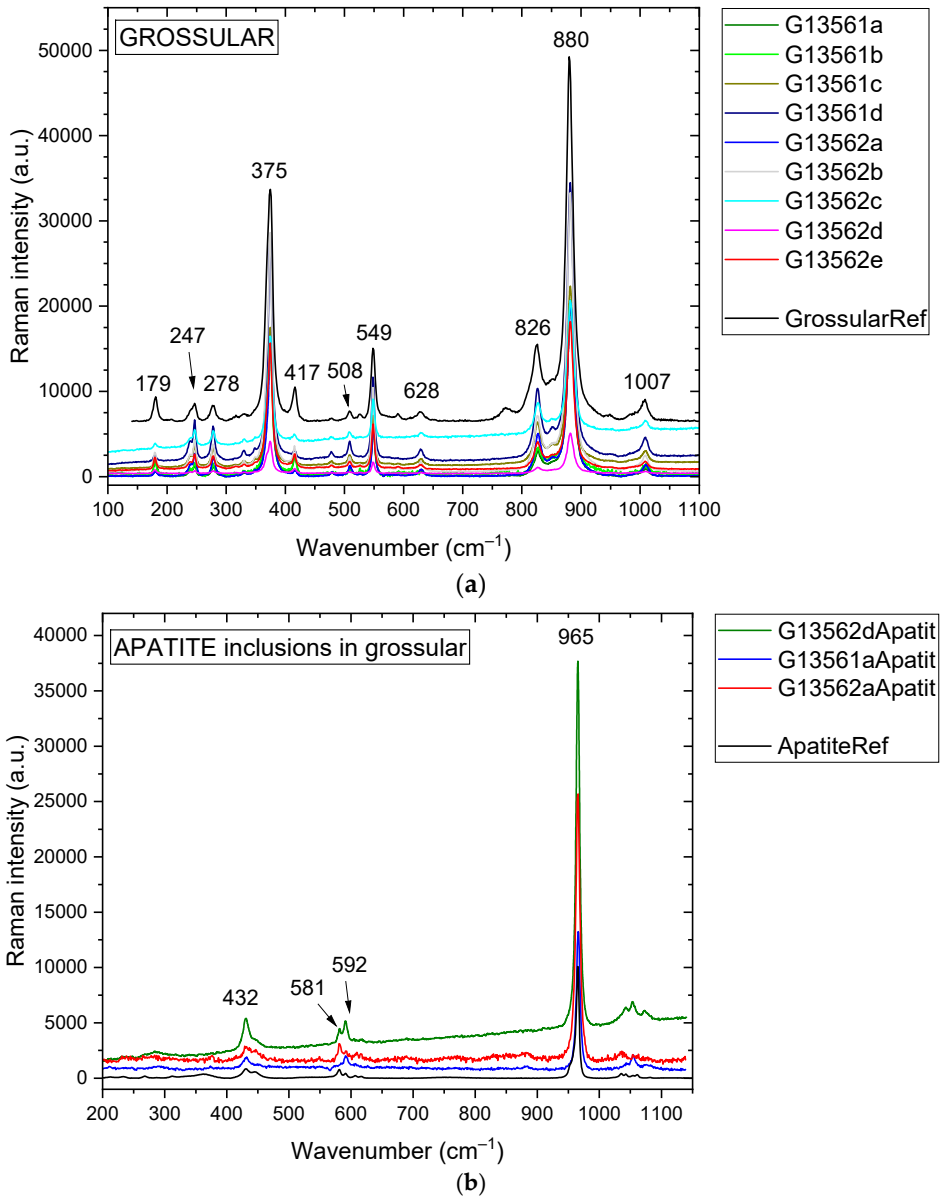

Figure 6. (**a**) Raman spectra from the gems identified as grossular. The spectrum used as a reference (black line) is n. R040065 from the RRUFF database [36]. (**b**) Raman spectra of one of the inclusions identified as apatite. The spectrum used as a reference (black line) is n. R050194 from the RRUFF database [36].

Chemical analyses of the garnets of the present study (Table S2) confirm their classification, with a grossular content exceeding 85 wt% (calculated using the Locock spreadsheet calculation [72]). The high FeO content (2.9–3.6 wt%) explains the cinnamon-red colour of the stones. Gemstones with these characteristics are commercially known as hessonite [73,74].

Grossular, and garnets in general, are rock-forming minerals, meaning that garnet deposits are common all over the globe. However, not all grossular specimens possess the characteristics suitable for gemstone cutting, such as transparency, crystal size, and colour [75]. Fortunately for this study, gem-quality cinnamon-red grossular (or hessonite) deposits are relatively rare. The most renowned gem-quality red grossular garnets are mined in India [76,77] and Sri Lanka [77–79]. Other documented and studied deposits are in Italy, Tanzania, and Mexico [80,81]; Russia [82] and Madagascar [83], with gemstones often

presenting a greenish hue; and the U.S.A. [84,85] and Canada [86–88], typically with small and fractured specimens. Recent discoveries have also been reported in Somaliland [89].

Chemical characterizations of this type of gemstone, like the one carried out by PIXE-PIGE, comprehensive of main, minor, and trace elements (Figure 7), are not very common. This is likely because the most commonly used method for classifying grossular gemstone is based on the optical properties of the stone [90]. Nevertheless, we can make several observations regarding the chemical and mineralogical composition of the garnets analysed in this study comparing them with the literature cited above.

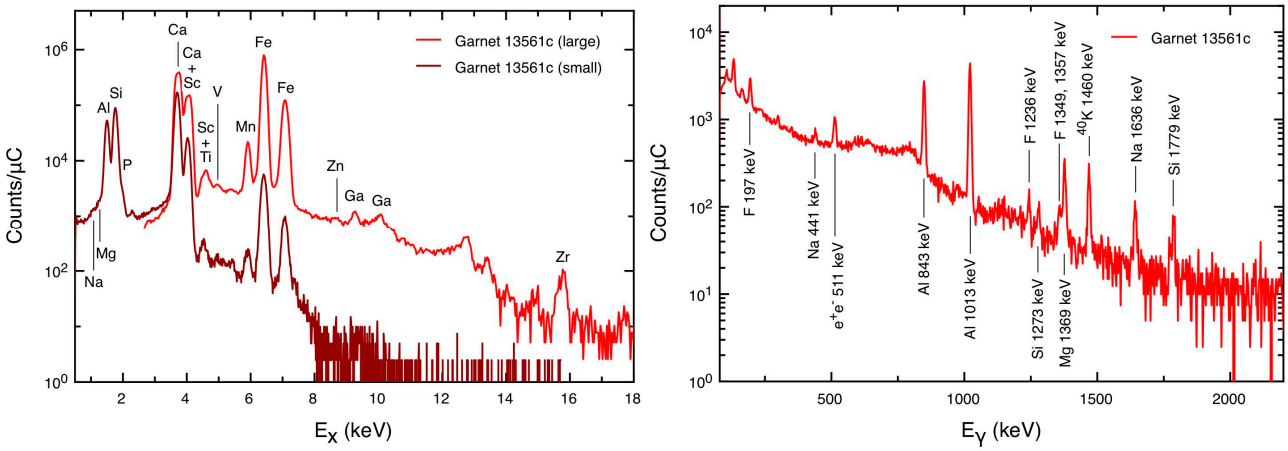

Figure 7. PIXE spectra obtained with the two detectors (**left**) and PIGE spectrum (**right**), all normalised to the collected beam charge, from a gem identified as grossular.

The studied grossulars are characterised by negligible amounts of MnO (~0.1 wt%), MgO (0.2–0.3 wt%), and NaO_2 (b.l.d. to 0.4 wt%). V and Cr are both below the detection limits of 32 and 27 ppm, respectively, while trace amounts of Ti (below detection at 269 ppm) and Zr (below detection at 29 ppm) are present. F is detected at 0.8–1.2 wt%. The most similar chemical profile found in the literature belongs to grossular garnets from Sri Lanka, which are among the few reported to contain F and exhibit very low Ti levels, with a comparable FeO content [78]. Orange-brown grossular garnets from Tanzania also appear to be compatible [80]. The fragmented and limited availability of chemical data in the literature, combined with the variability in chemical composition exhibited by these gemstones, makes a definitive attribution challenging. However, another factor supporting the attribution of these garnets to Sri Lankan deposits is the presence of apatite inclusions, identified as characteristic of these gemstones by Zwaan [79]. This provenance aligns with the quality of the gemstones in this study, which are clear, free of fractures, and of good gem quality. Finally, it is well known that one of the oldest trade routes, dating back to the Roman period, involved high-quality garnets used as gemstones, originating specifically from the deposits in Sri Lanka [91].

It is interesting to note that the cuts of these gemstones display unusual shapes, not comparable to standardised forms (Figure 1). Cuts like those seen in these grossular specimens have similarities with pieces from the 17th century, when gemstone cutting styles had not yet been fully standardised.

3.4. Cordierite

Cordierite is a mineral with a complex chemical formula, idealised as $(Mg,Fe)_2[Al_4,Si_5,O_{18}]^*$ (H_2O, CO_2). The crystal structure of cordierite is complex and belongs to the cyclosilicate based on a ring-like structure of linked tetrahedra of SiO_4 and AlO_4. The octahedral site

can contain Mg^{2+}, Fe^{2+}, and Mn^{2+}. The channels formed by the tetrahedra rings can hold molecules of H_2O and CO_2 and other small ions like alkali metals [92,93].

None of the analysed gems were classified as cordierite in the museum catalogue, but according to the analytical results, eleven gems listed as amethyst quartz were actually cordierites (Table 1).

The identification was carried out by micro-Raman analysis (Figure 8a), with the main bands at 972 and 1012 cm^{-1}, relative to the stretching mode of SiO_4 tetrahedra. The Raman spectrum of cordierite reflects the complexity of the crystal structure of the species. The bands in the lowest part of the spectrum below 428 cm^{-1} are mainly related to the bending of various tetrahedra sites accompanied also with the bending of an Al tetrahedral site (241 cm^{-1} and 295 cm^{-1}) and octahedral site (bands at 241, 327, and 556 cm^{-1}) [94,95].

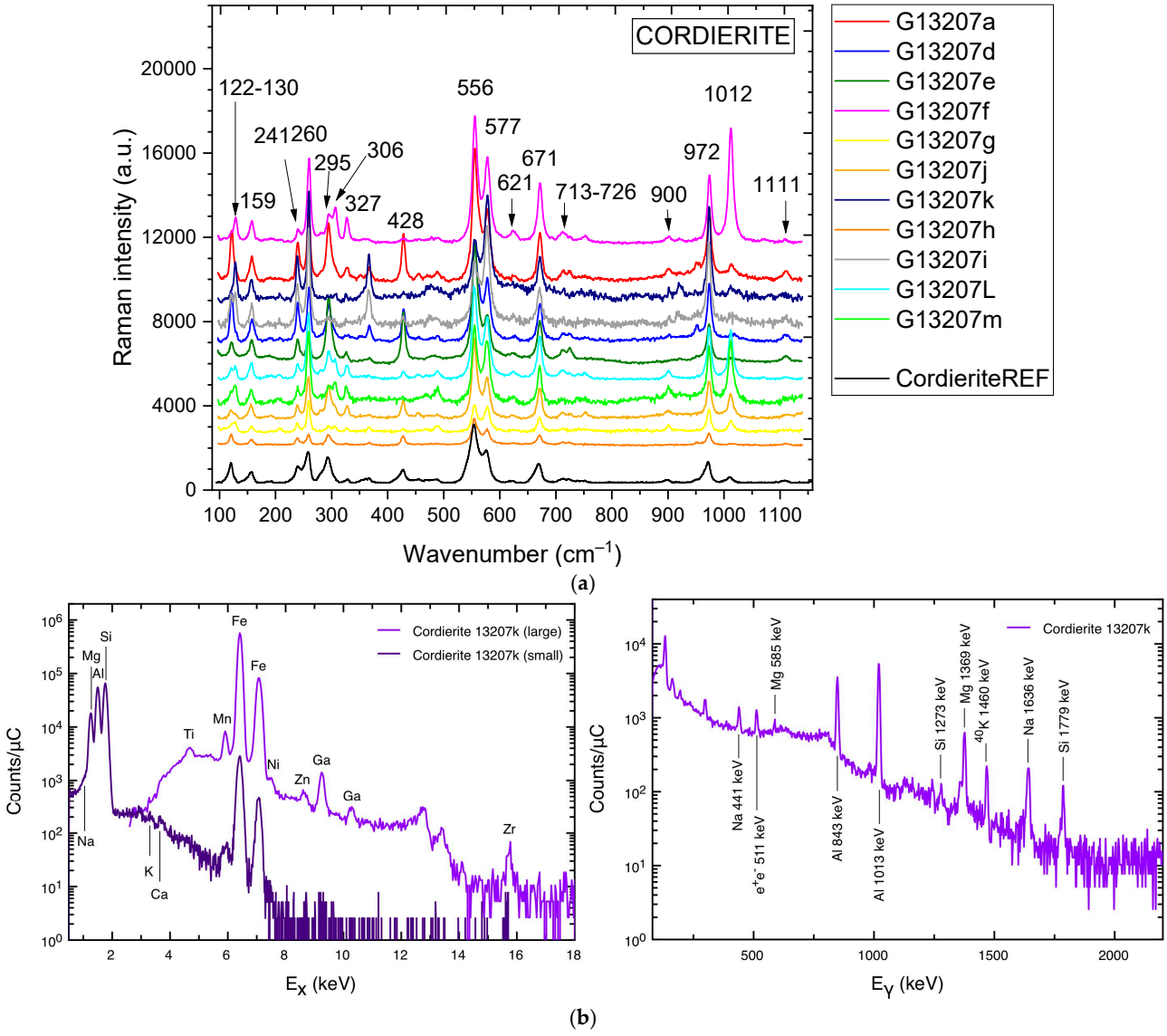

Figure 8. (**a**) Raman spectra from the gems identified as cordierite. The spectrum used as a reference (black line) is n. R040081 from the RRUFF database [36]. (**b**) PIXE spectra obtained with the two detectors (**left**) and PIGE spectrum (**right**), all normalised to the collected beam charge, from a gem identified as cordierite.

Bands in the range 556–726 cm^{-1} can be assigned to stretching and bending modes of both tetrahedral and octahedral sites. In particular, the visible separation of bands at 556 and 577 cm^{-1} is significant because it could indicate an extensive ordering of the Al-Si

distribution within the tetrahedra in an orthorhombic structure and the consequent belonging of these specimens at the low-temperature cordierites [94]. The partial substitution of Mg^{2+} with Fe^{2+} in the octahedral sites appears to have a dual effect: shifting several bands to lower values compared to the spectrum of ideal Mg cordierites and widening the gap between values just below 800 cm^{-1} and 900 cm^{-1} [94,95]. These phenomena are observed in the spectra of the investigated specimens. Finally, stretching vibrations of the tetrahedral sites prevail in the bands above 900 cm^{-1} [94,95].

Since cordierite is a rock-forming mineral, it can be found in numerous deposits. However, also in this case, deposits providing gem-quality specimens of this mineral are far fewer [96]. Gemmological and chemical studies on gem-quality cordierite are rare, but deposits of this kind are documented in Madagascar [96], Tanzania, Zimbabwe [92,97], U.S.A (Wyoming) [98,99], Canada [100], Czech Republic [101], and, the most famous ones, India [102,103] and Sri Lanka [79,104].

The chemical data obtained in this study (Figure 8b and Table S2) were compared with chemical data from cordierites originating from gem-producing countries of the same type. Given the limited data available in the literature, the chemical data used for comparison do not always come from gems (see Figure 9). Comparing the major and minor component compositions reveals how the specimens have a medium–low amount of FeO, while the MgO content is medium–high. This is consistent with other beautiful specimens analysed in a previous study [93] and explains the intense colour and strong pleochroism displayed by the analysed gems. Gems with these characteristics are commercially known and often classified as Iolite [93].

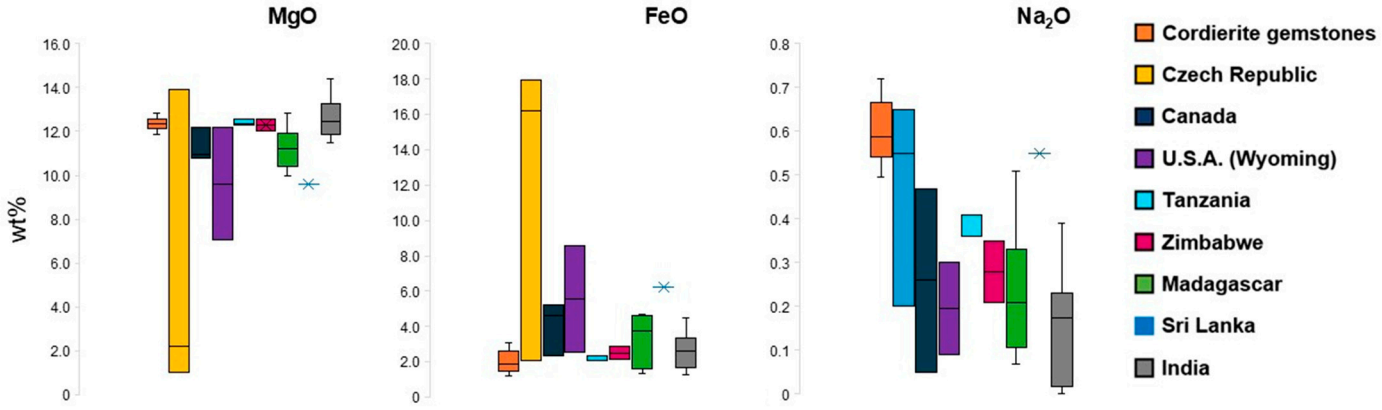

Figure 9. Distribution of MgO, FeO, and Na_2O content in the cordierites of this study, compared to those of other countries producing gem-quality cordierite: Czech Republic (museum-quality samples from Dolní Bory [92,105]); Canada (gem-quality cordierite from Thor-Odin Dome, British Columbia [100], and mineralogical sample from SE Ontario [106]); U.S.A. (rock samples from Laramie Range, Albany [92,99]); Tanzania (gem-quality sample from [92] and museum-quality samples from [105]); Zimbabwe (gem-quality sample from [92] and mineral sample from [105]); Madagascar (museum samples, one from Manivitsy, the other from an unknown locality [106], and gem-quality samples [96]); Sri Lanka (only one rock specimen from Colombo [92], labelled with a bar covered with X symbol); and India (gem-quality samples from Kalahandi, Odisha [94,103], mineralogical samples from Kiranur S-India [92], Ganguvarpatti [106], and Ellammankovilpatti, Tamil Nadu [106,107]).

As shown in Figure 9, the composition of major and minor elements of minerals from different origins exhibit numerous overlaps, making it impossible to distinguish between deposits. The trace elements content of the analysed gems is presented in Table S2. Cordierites from this study are characterised by the presence of low Ti (<26 ppm), Ga (<64 ppm), Rb (<27 ppm), and Zn (<27 ppm) content. The lack of systematic studies on the trace elements composition of these gems prevents comparisons with our study's data

with those from other deposits. Promising elements for further investigation could include Be and Li (below the detection limit in our study; see Table S1), involved in the dominant substitution mechanisms observed in the species [92], as well as CO_2 and H_2O content, which cannot be measured using the methods of the present study.

It can be concluded that, as far as is known, Canadian and American deposits of this gemstone were discovered in the last 50–70 years [98,100], African deposits are poorly documented and studied [97], and those in the Czech Republic are not particularly productive [101]. The most plausible hypothesis remains that the cordierites in this study originate from an Indian or Sri Lankan deposit, known since ancient times [108].

3.5. Quartz

Quartz is the most represented mineralogical species in this set of gems. This is not surprising as it is also the most prevalent mineral within the museum's collection of Carved Stone [4]. What is remarkable, however, is the abundance of quartz varieties, ranging from macrocrystalline to cryptocrystalline structures. This likely reflects a strong appreciation for this material at the time that the collection was assembled (before 1793).

The identification of the mineralogical species was carried out through micro-Raman analysis using the main bands characteristic of α-quartz: 127, 208, 353, and 465 cm^{-1} [109] (Figure 10a). However, the technique does not distinguish between macrocrystalline and microcrystalline quartz [109,110], nor does it seem to differentiate between different coloured quartz varieties [111]. Nevertheless, this discrimination was possible in some cases based on the colour and pattern observable on the gemstones. Violet quartz specimens can be classified as amethysts (samples 13207c, 13207n, and 13207o, correctly catalogued in the museum records), while a grey quartz gemstone appears to be smoky quartz (13207b), although it was catalogued as amethyst. Pale yellow quartz samples (13158, 13182, 13541a, 13541b, 13539b) are likely citrine quartz or possibly heat-treated amethysts [112]; among them, only two samples, 13158 and 13182, were correctly catalogued as quartz, while the others were mistakenly catalogued as topaz (Table 1). Regarding the microcrystalline quartz specimens, sample 13333 exhibits the red colour characteristic of the semi-precious gemstone known as carnelian [113]. Samples 13355a and 13355b display the typical concentric colourful bands of agate [113], while mint-green sample 13601c was incorrectly classified as emerald in the catalogue. This last specimen has an appearance compatible with that of chrysoprase, and its Raman spectrum shows the band at 502 cm^{-1} attributed to moganite inclusions [110], which are common in this type of semi-precious gemstone. However, to confidently attribute the specimen to this gemstone type, its Ni content should be determined [110].

Some of the quartz specimens have inclusions visible to the naked eye. Sample 13161 features rutile inclusions (Figure 10b), identified by bands at 145, 238, 448, and 613 cm^{-1} in the Raman spectra [114]. Samples 13165, 13177, and 13394 (Figure 10b) contain hematite inclusions, recognised by the bands at 226, 293, 412, 500, and 613 cm^{-1} [33]. Additionally, sample 13403a has remarkable dendritic inclusions primarily composed of iron and manganese oxides.

Two quartz specimens (13172 and 13199) exhibit unique characteristics identified during the autoptic analysis (Figure 1). Sample 13199 displays an unnatural, artificial coloration. Sample 13172 was recognised in this study as a replica of the famous Regent Diamond, currently state property of France and housed in the Louvre Museum, since it has the same cut. The existence of this replica, made of quartz in its transparent form (hyaline quartz) is documented in record nr. 59 filza XV dated 1782, now preserved in the Historical Archive and Research Department of the Uffizi Gallery [115]. The artefact was among the pieces selected for transfer from the Uffizi Gallery to the newly established Imperial and

Royal Museum of Physics and Natural History by the Grand Duke's Private Secretary. The document proves that the gem was already present in the Uffizi Gallery collection prior to the transfer. Further historical investigations will be conducted on this topic.

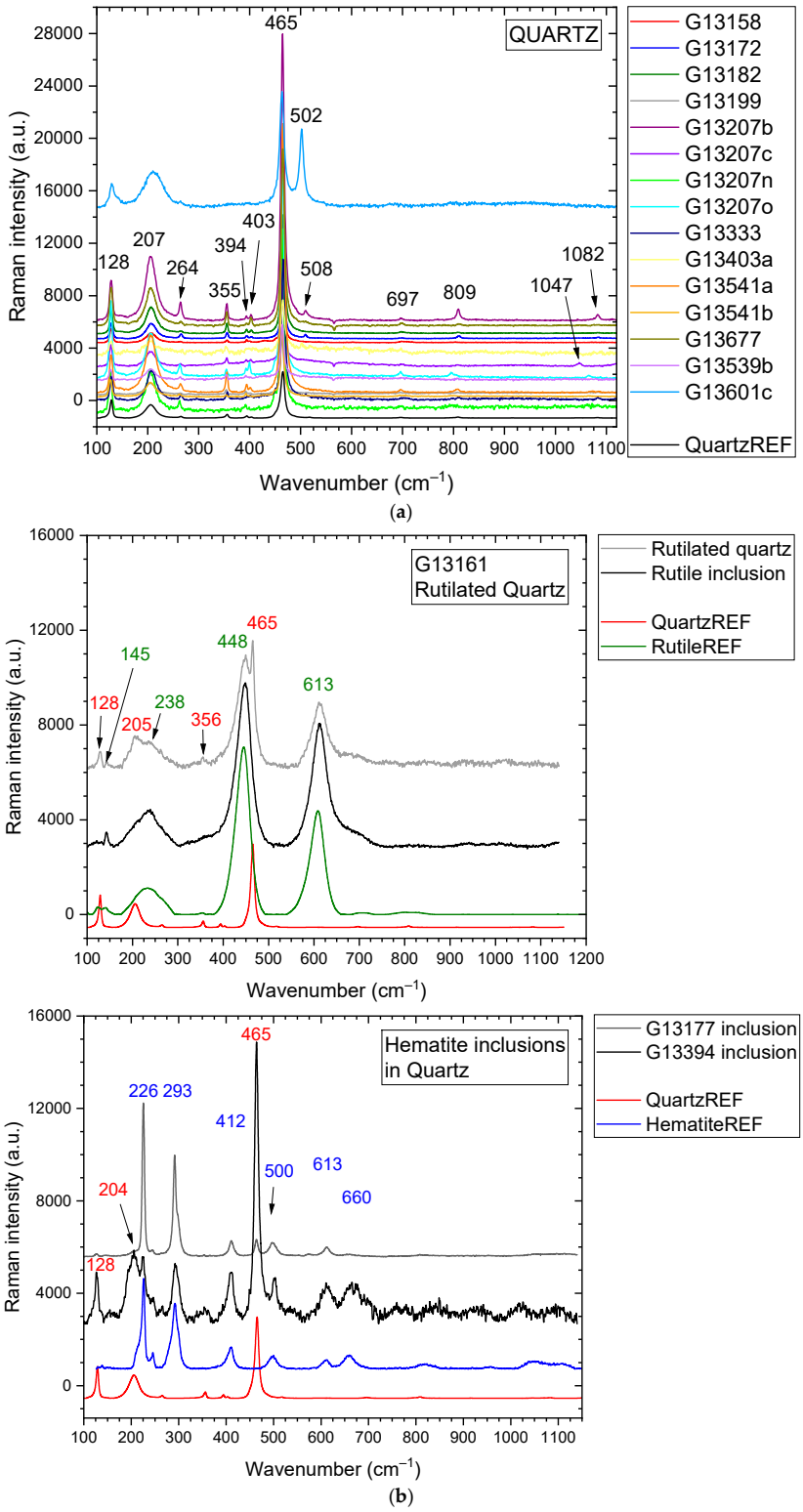

Figure 10. (**a**) Raman spectra from the gems identified as quartz. The spectrum used as a reference (black line) is n. X080015 from the RRUFF database. (**b**) Raman spectra from the quartz gems in which rutile (**top**) and hematite (**bottom**) inclusions were identified. The spectra from the RRUFF database [36] used as a reference are n. X080015 for quartz (red line), R050300 for hematite (blue line), and R060493 for rutile (green line).

Chemical compositions of tree specimens are reported in Table S2. As expected, all quartz samples show a SiO_2 content above 98.9 wt%, being one of the minerals with the lowest content of chemical impurities [116]. Al_2O_3 is one of the most common impurities, and in our samples, it also appears in a range of 0.6–0.7 wt%. The amount of Na_2O (0.1–0.5 wt% in our samples) is usually related to fluid inclusions [116]. Fe content, which is related to the colouration of the gemstones [116] is 57 ppm in the violet amethyst quartz and 70 ppm in the grey smoky quartz. In the artificially coloured sample, the Fe amount is of 76 ppm. Samples 13207b and 13207o show higher Ti content than 13199. Ti content in quartz seem to be related to the formation environment of the mineral, and it is higher in quartz from magmatic rocks and lower in hydrothermal environments [116]. A similar consideration can be made for Ge, b.l.d. in 13199, ranging between 7 and 11 ppm in the other samples. Quartz from granitic and pegmatitic magmas show higher Ge content than other quartzes [116].

Ga trace amounts are common in quartz, but their typical amounts are debated in the literature [116]. Amethyst 13207o has 7 ppm of Ga; the smoky quartz, 14 ppm; and sample 13199 is b.l.d. P content is generally low in quartz [116], unlike in the sample studied, which reached 1198 ppm in sample 13207o (amethyst).

It is interesting to note that the artificially coloured sample exhibits an unusual sulphur content, possibly linked to processing with acidic substances [117]. However, the available data are insufficient to determine the specific type of treatment involved.

3.6. Other Gemstones and Glass

The catalogue classification of sample 13678 as orthoclase is confirmed by its Raman spectrum (Figure 11), showing the characteristic bands at 153, 284, 477, and 514 cm^{-1} [118]. In contrast, sample 13706, labelled as spinel in the museum catalogue, was identified as a stunning tourmaline. It exhibits the typical banded pleochroism of this mineralogical species, with two bright pink shades. The spectrum of the sample (Figure 12) shows bands at 222, 377, 729, and 1065 cm^{-1} and is compatible with rose specimens of elbaite [119].

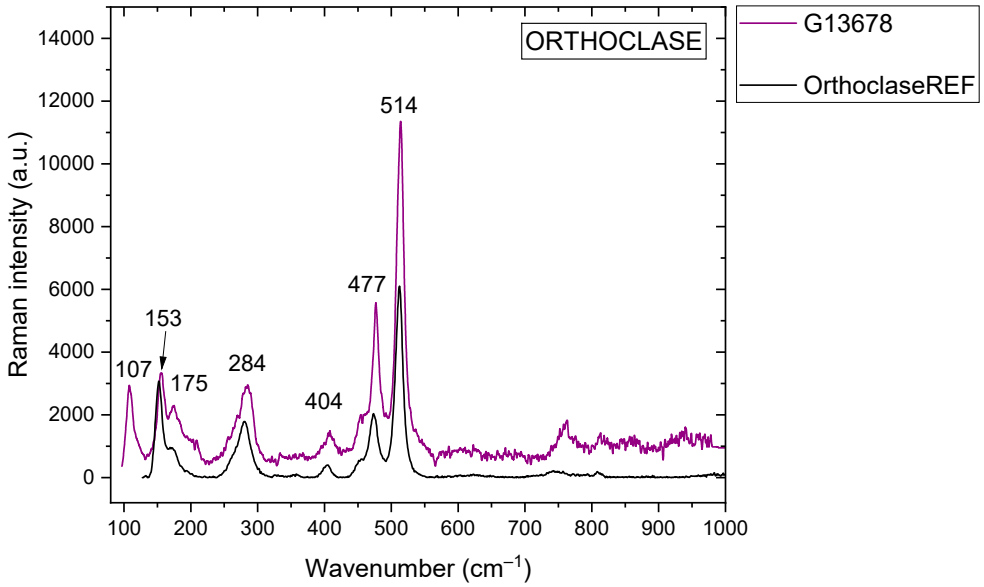

Figure 11. Raman spectrum from the gem identified as orthoclase. The spectrum used as a reference (black line) is n. R040055 from the RRUFF database [36].

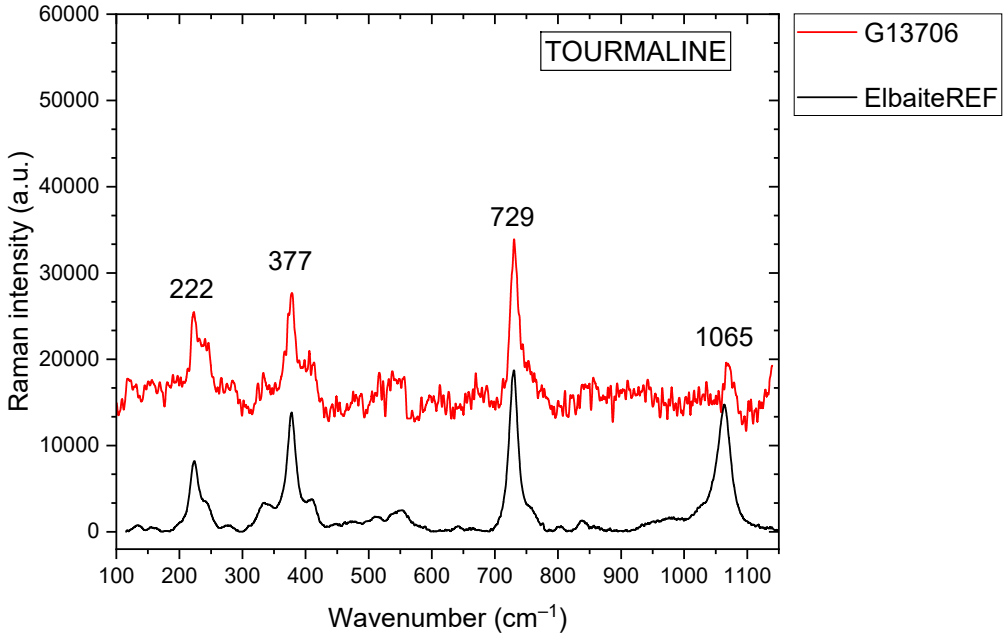

Figure 12. Raman spectrum from the gem identified as tourmaline. The spectrum used as a reference (black line) is n. R050260 from the RRUFF database [36].

Finally, this splendid collection could not lack a forgery: sample 13550, labelled as garnet, was identified as glass (Figure 13). Its chemical composition, including SiO_2, K_2O, Na_2O, B_2O_3, and As_2O_5 (Table S2), is consistent with that of 17th century North Bohemian glasses [120]. The low MgO content (~1.2 wt%) and the absence of P (b.d.l.), combined with the presence of As_2O_3, suggest that the glass was likely produced from batches containing potash (and/or saltpetre) as a flux, along with arsenic and other components. Another relevant factor is the low CaO content, which is characteristic of this type of manufacture (while increased in later productions of crystal and white glass). The use of saltpetre and arsenic in the production of certain types of glass in Central Europe likely began not earlier than the second half of the 17th century [120].

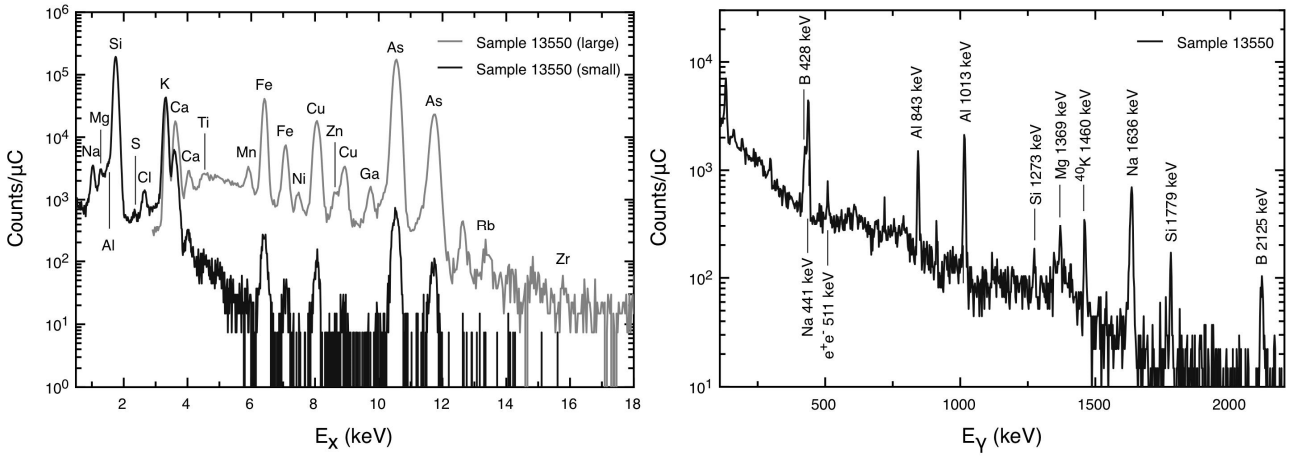

Figure 13. PIXE spectra obtained with the two detectors (**left**) and PIGE spectrum (**right**), all normalised to the collected beam charge, from the fake gem labelled as garnet, but identified as glass.

4. Conclusions

Fifty gemstones from the Carved Stone Collection of the La Specola Museum in Florence (Italy) were studied using micro-Raman and PIXE-PIGE techniques, yielding mineralogical and chemical data. The set of samples belongs to the original core of the

collection, as all specimens appear in the first catalogue dated 1793. For this reason, it is reasonable to hypothesise that they originated from the Medici House, which initiated the collection of materials now preserved in the museum.

The mineralogical classification of twenty-nine out of the fifty analysed samples, as reported in the most up-to-date catalogue from 1943/1947, has been revised. The mineralogical and chemical data obtained have been used to improve the understanding of the gemstones' provenance and origins. The most significant findings can be summarised as follows:

1. The trace element composition of the emeralds in the collection shows greater compatibility with emeralds from Colombia than those from Brazil, despite the latter being the origin stated on the label.
2. The topazes are likely of hydrothermal origin, as indicated by their F content. The trace element composition of the intensely yellow specimens appears to be compatible with Brazilian deposits.
3. The deep cinnamon colour, along with the FeO and F contents and the presence of apatite inclusions in the nine grossular gemstones, allows them to be identified as hessonite and linked to the Sri Lanka deposits.
4. The cordierite nature of 11 gemstones, not listed in the ancient catalogue, has been identified. Historical considerations suggest that the most likely origin of these samples is India or Sri Lanka. However, a higher number of chemical analyses of gem-quality samples would be helpful to confirm or refute this hypothesis.
5. A fake gemstone, sample 13550, is made of glass rich in K_2O, B_2O_3, and As_2O_5. This distinctive composition could associate the sample with the North Bohemian glass production of the 17th century, linking it to the period of Medici House ownership.
6. Sample 13172, made of hyaline quartz, was identified as a replica of the Regent Diamond, previously housed in the Uffizi Gallery and later transferred by the Private Secretary of Grand Duke Peter Leopold in 1782 to its current location.

It is important to emphasise that, given the significance and value of the gemstones, the analyses were conducted using entirely non-invasive techniques. This approach provided data and information typically obtained through destructive or micro-destructive methods, such as in determining the Be and F content, which is essential for provenance studies of gemstones.

Supplementary Materials: The following supporting information can be downloaded at https://www.mdpi.com/article/10.3390/min15020096/s1: Table S1: Limits of detection of the PIXE-PIGE analysis; Table S2: PIXE-PIGE quantitative results.

Author Contributions: Methodology, L.F.; formal analysis, L.F.; investigation, L.F., M.C. and V.M.C.; data curation, L.F., M.C. and R.M.; writing—original draft preparation, L.F.; writing—review and editing, L.F., M.C., R.M. and M.B.; supervision, M.B. All authors have read and agreed to the published version of the manuscript.

Funding: This research was funded by University Museums System of University of Florence (Firenze, Italy).

Data Availability Statement: The original contributions presented in this study are included in the article/Supplementary Materials. Further inquiries can be directed to the corresponding author.

Acknowledgments: The authors sincerely wish to thank Luciana Fantoni for the historical research conducted on the collection, Marilena Ricci for the Raman analyses carried out at the Department of Chemistry's "Ugo Schiff" laboratory, Costanza Bronconi for her thesis work on this topic, Fausto Barbagli for his assistance in understanding the historical context in which the collection was formed,

and Asami Hirata and Riccardo Gennaioli for offering their expertise in the identification of gemstone cuts.

Conflicts of Interest: The authors declare no conflict of interest.

References

1. Luchinat, C.A.; Sframeli, M. *Magnificenza alla Corte dei Medici: Arte a Firenze Alla Fine Del Cinquecento*; Electa: Milan, Italy, 1997; ISBN 978-88-435-6217-6.
2. Cesati, F. *The Medici: Story of a European Dynasty*; Information and Interdisciplinary Subjects Series; Mandragora: Florence, Italy, 1999; ISBN 978-88-85957-36-7.
3. Contardi, S. *La Casa di Salomone a Firenze: L'imperiale e Reale Museo di Fisica e Storia Naturale, 1775–1801*; Biblioteca di Nuncius; L.S. Olschki: Florence, Italy, 2002; ISBN 978-88-222-5092-6.
4. Fantoni, L.; Poggi, L. La Collezione di Pietre Lavorate. In *Museum of Natural History of the University of Florence. The Mineralogical and Lithological Collections/a cura di Giovanni Pratesi*; Firenze University Press: Florence, Italy, 2012; Volume 4, pp. 55–65, ISBN 978-88-6655-319-9.
5. Cipriani, C.; Fantoni, L.; Poggi, L.; Scarpellini, A. *Le Collezioni Mineralogiche del Museo di Storia Naturale dell'Università di Firenze dalle Origini a Oggi*; Leo S. Olschki: Florence, Italy, 2011; ISBN 88-222-6002-3.
6. Barbagli, F. Genesi e Sviluppo Delle Collezioni. In *The Museum of Natural History of the University of Florence: The Collections of la specola: Zoology and anatomical Waxes/a cura di Giulio Barsanti e Guido Chelazzi*; Firenze University Press: Florence, Italy, 2009; Volume 1, pp. 257–277, ISBN 978-88-8453-848-2.
7. Bouchard, M.; Smith, D.C. Catalogue of 45 Reference Raman Spectra of Minerals Concerning Research in Art History or Archaeology, Especially on Corroded Metals and Coloured Glass. *Spectrochim. Acta Part A Mol. Biomol. Spectrosc.* **2003**, *59*, 2247–2266. [CrossRef] [PubMed]
8. Mazzoleni, P.; Barone, G.; Raneri, S.; Aquilia, E.; Bersani, D.; Cirrincione, R. Application of Micro-Raman Spectroscopy for the Identification of Unclassified Minerals Preserved in Old Museum Collections. *Plinius* **2016**, *42*, 112–124. [CrossRef]
9. Barone, G.; Bersani, D.; Lottici, P.P.; Mazzoleni, P.; Raneri, S.; Longobardo, U. Red Gemstone Characterization by Micro-Raman Spectroscopy: The Case of Rubies and Their Imitations. *J. Raman Spectrosc.* **2016**, *47*, 1534–1539. [CrossRef]
10. Bruni, Y.; Hatert, F.; George, P.; Cambier, H.; Strivay, D. A Gemmological Study of the Reliquary Crown of Namur, Belgium. *Eur. J. Miner.* **2021**, *33*, 221–232. [CrossRef]
11. Barone, G.; Bersani, D.; Jehlička, J.; Lottici, P.P.; Mazzoleni, P.; Raneri, S.; Vandenabeele, P.; Di Giacomo, C.; Larinà, G. Nondestructive Investigation on the 17–18th Centuries Sicilian Jewelry Collection at the Messina Regional Museum Using Mobile Raman Equipment. *J. Raman Spectrosc.* **2015**, *46*, 989–995. [CrossRef]
12. Barone, G.; Mazzoleni, P.; Raneri, S.; Jehlička, J.; Vandenabeele, P.; Lottici, P.P.; Lamagna, G.; Manenti, A.M.; Bersani, D. Raman Investigation of Precious Jewelry Collections Preserved in Paolo Orsi Regional Museum (Siracusa, Sicily) Using Portable Equipment. *Appl. Spectrosc.* **2016**, *70*, 1420–1431. [CrossRef]
13. Pappalardo, L.; Karydas, A.G.; Kotzamani, N.; Pappalardo, G.; Romano, F.P.; Zarkadas, C. Complementary Use of PIXE-Alpha and XRF Portable Systems for the Non-Destructive and in Situ Characterization of Gemstones in Museums. *Nucl. Instrum. Methods Phys. Res. Sect. B Beam Interact. Mater. At.* **2005**, *239*, 114–121. [CrossRef]
14. Perea, A.; Climent-Font, A.; Fernández-Jiménez, M.; Enguita, O.; Gutiérrez, P.C.; Calusi, S.; Migliori, A.; Montero, I. The Visigothic Treasure of Torredonjimeno (Jaén, Spain): A Study with IBA Techniques. *Nucl. Instrum. Methods Phys. Res. Sect. B Beam Interact. Mater. At.* **2006**, *249*, 638–641. [CrossRef]
15. Ontalba Salamanca, M.Á.; Gómez Tubío, B.; de la Bandera, M.L.; Respaldiza, M.Á. PIXE–PIGE Analysis of a Visigothic Gold Cross. *Nucl. Instrum. Methods Phys. Res. Sect. B Beam Interact. Mater. At.* **2004**, *226*, 199–207. [CrossRef]
16. Calligaro, T.; Mossmann, A.; Poirot, J.-P.; Querré, G. Provenance Study of Rubies from a Parthian Statuette by PIXE Analysis. *Nucl. Instrum. Methods Phys. Res. Sect. B Beam Interact. Mater. At.* **1998**, *136–138*, 846–850. [CrossRef]
17. Yu, K.N.; Tang, S.M.; Tay, T.S. PIXE Studies of Emeralds. *X-Ray Spectrom.* **2000**, *29*, 267–278. [CrossRef]
18. Abdel Gawad, A.E.; Ene, A.; Skublov, S.G.; Gavrilchik, A.K.; Ali, M.A.; Ghoneim, M.M.; Nastavkin, A.V. Trace Element Geochemistry and Genesis of Beryl from Wadi Nugrus, South Eastern Desert, Egypt. *Minerals* **2022**, *12*, 206. [CrossRef]
19. Calligaro, T.; Dran, J.-C.; Poirot, J.-P.; Querré, G.; Salomon, J.; Zwaan, J.C. PIXE/PIGE Characterisation of Emeralds Using an External Micro-Beam. *Nucl. Instrum. Methods Phys. Res. Sect. B Beam Interact. Mater. At.* **2000**, *161–163*, 769–774. [CrossRef]
20. Venkateswarulu, P.; Srinivasa Rao, K.; Kasipathi, C.; Ramakrishna, Y. Multielemental Analyses of Isomorphous Indian Garnet Gemstones by XRD and External Pixe Techniques. *Appl. Radiat. Isot.* **2012**, *70*, 2746–2754. [CrossRef]
21. Vaggelli, G.; Borghi, A.; Cossio, R.; Mazzoli, C.; Olmi, F. Comparison between Major and Trace Element Concentrations in Garnet Performed by EPMA and Micro-PIXE Techniques. *Spectrochim. Acta Part B At. Spectrosc.* **2003**, *58*, 699–709. [CrossRef]

22. Mathis, F.; Vrielynck, O.; Laclavetine, K.; Chêne, G.; Strivay, D. Study of the Provenance of Belgian Merovingian Garnets by PIXE at IPNAS Cyclotron. *Nucl. Instrum. Methods Phys. Res. Sect. B Beam Interact. Mater. At.* **2008**, *266*, 2348–2352. [CrossRef]
23. Borghi, A.; Cossio, R.; Mazzoli, C. A Mineralogical Application of Micro-PIXE Technique: Yttrium Zoning in Garnet from Metamorphic Rocks and Its Petrologic Meaning. *Nucl. Instrum. Methods Phys. Res. Sect. B Beam Interact. Mater. At.* **2002**, *189*, 412–417. [CrossRef]
24. Venkateswara Rao, R.; Venkateswarulu, P.; Kasipathi, C.; SivaJyothi, S. Trace Elemental Analysis of Indian Natural Moonstone Gems by PIXE and XRD Techniques. *Appl. Radiat. Isot.* **2013**, *82*, 211–222. [CrossRef] [PubMed]
25. Chulapakorn, T.; Intarasiri, S.; Bootkul, D.; Singkarat, S. Identification of Deposit Types of Natural Corundum by PIXE. *Nucl. Instrum. Methods Phys. Res. Sect. B Beam Interact. Mater. At.* **2014**, *331*, 108–112. [CrossRef]
26. Chiari, M.; Barone, S.; Bombini, A.; Calzolai, G.; Carraresi, L.; Castelli, L.; Czelusniak, C.; Fedi, M.E.; Gelli, N.; Giambi, F.; et al. LABEC, the INFN Ion Beam Laboratory of Nuclear Techniques for Environment and Cultural Heritage. *Eur. Phys. J. Plus* **2021**, *136*, 472. [CrossRef] [PubMed]
27. Chiari, M. External Beam IBA Measurements for Cultural Heritage. *Appl. Sci.* **2023**, *13*, 3366. [CrossRef]
28. Chiari, M.; Migliori, A.; Mandò, P.A. Measurement of Low Currents in an External Beam Set-Up. *Nucl. Instrum. Methods Phys. Res. Sect. B Beam Interact. Mater. At.* **2002**, *188*, 162–165. [CrossRef]
29. Campbell, J.L.; Boyd, N.I.; Grassi, N.; Bonnick, P.; Maxwell, J.A. The Guelph PIXE Software Package IV. *Nucl. Instrum. Methods Phys. Res. Sect. B Beam Interact. Mater. At.* **2010**, *268*, 3356–3363. [CrossRef]
30. Pessoa Barradas, N.; Cruz, J.; Fonseca, M.; de Jesus, A.P.; Lagoyannis, A.; Manteigas, V.; Mayer, M.; Preketes-Sigalas, K.; Dimitriou, P. International Atomic Energy Agency Inter-Comparison of Particle Induced Gamma-Ray Emission Codes for Bulk Samples. *Nucl. Instrum. Methods Phys. Res. Sect. B Beam Interact. Mater. At.* **2020**, *468*, 37–47. [CrossRef]
31. Bachiller Perea, D.; Corvisiero, P.; Jiménez Rey, D.; Joco, V.; Maira Vidal, A.; Muñoz Martin, A.; Zucchiatti, A. Measurement of Gamma-Ray Production Cross Sections in Li and F Induced by Protons from 810 to 3700 keV. *Nucl. Instrum. Methods Phys. Res. Sect. B Beam Interact. Mater. At.* **2017**, *406*, 161–166. [CrossRef]
32. Moroz, I.; Roth, M.; Boudeulle, M.; Panczer, G. Raman Microspectroscopy and Fluorescence of Emeralds from Various Deposits. *J. Raman Spectrosc.* **2000**, *31*, 485–490. [CrossRef]
33. Culka, A.; Jehlička, J. A Database of Raman Spectra of Precious Gemstones and Minerals Used as Cut Gems Obtained Using Portable Sequentially Shifted Excitation Raman Spectrometer. *J. Raman Spectrosc.* **2019**, *50*, 262–280. [CrossRef]
34. Bersani, D.; Azzi, G.; Lambruschi, E.; Barone, G.; Mazzoleni, P.; Raneri, S.; Longobardo, U.; Lottici, P.P. Characterization of Emeralds by Micro-Raman Spectroscopy. *J. Raman Spectrosc.* **2014**, *45*, 1293–1300. [CrossRef]
35. Lafuente, B.; Downs, R.T.; Yang, H.; Stone, N.; Armbruster, T.; Danisi, R.M. The Power of Databases: The RRUFF Project. *Highlights Mineral. Crystallogr.* **2015**, *1*, 25.
36. RRUFF Database. Available online: https://rruff.info/ (accessed on 26 August 2024).
37. Chen, Q.; Bao, P.; Li, Y.; Shen, A.H.; Gao, R.; Bai, Y.; Gong, X.; Liu, X. A Research of Emeralds from Panjshir Valley, Afghanistan. *Minerals* **2023**, *13*, 63. [CrossRef]
38. Guo, H.; Yu, X.; Zheng, Y.; Sun, Z.; Ng, M.F.-Y. Inclusion and Trace Element Characteristics of Emeralds from Swat Valley, Pakistan. *Gems Gemol.* **2020**, *56*, 336–355. [CrossRef]
39. Karampelas, S.; Al-Shaybani, B.; Mohamed, F.; Sangsawong, S.; Al-Alawi, A. Emeralds from the Most Important Occurrences: Chemical and Spectroscopic Data. *Minerals* **2019**, *9*, 561. [CrossRef]
40. Zwaan, J.C. Gemmology, Geology and Origin of the Sandawana Emerald Deposits, Zimbabwe. *Scr. Geol.* **2006**, *131*, 1–212.
41. Zwaan, J.; Jacob, D.E.; Häger, T.; Neto, M.T.; Kanis, J. Emeralds from the Fazenda Bonfim Region, Rio Grande Do Norte, Brazil. *Gems Gemol.* **2012**, *48*, 2–17. [CrossRef]
42. Aurisicchio, C.; Conte, A.M.; Medeghini, L.; Ottolini, L.; De Vito, C. Major and Trace Element Geochemistry of Emerald from Several Deposits: Implications for Genetic Models and Classification Schemes. *Ore Geol. Rev.* **2018**, *94*, 351–366. [CrossRef]
43. Araújo, J.F.d.; Barreto, S.d.B.; Carrino, T.A.; Müller, A.; Santos, L.C.M.d.L. Mineralogical and Gemological Characterization of Emerald Crystals from Paraná Deposit, NE Brazil: A Study of Mineral Chemistry, Absorption and Reflectance Spectroscopy and Thermal Analysis. *Braz. J. Geol.* **2019**, *49*, e20190014. [CrossRef]
44. Zheng, Y.; Yu, X.; Guo, H. Major and Trace Element Geochemistry of Dayakou Vanadium-Dominant Emerald from Malipo (Yunnan, China): Genetic Model and Geographic Origin Determination. *Minerals* **2019**, *9*, 777. [CrossRef]
45. Alonso-Perez, R.; Day, J.M.D.; Pearson, D.G.; Luo, Y.; Palacios, M.A.; Sudhakar, R.; Palke, A. Exploring Emerald Global Geochemical Provenance through Fingerprinting and Machine Learning Methods. *Artif. Intell. Geosci.* **2024**, *5*, 100085. [CrossRef]
46. Giuliani, G.; Groat, L.A.; Marshall, D.; Fallick, A.E.; Branquet, Y. Emerald Deposits: A Review and Enhanced Classification. *Minerals* **2019**, *9*, 105. [CrossRef]
47. Saeseaw, S.; Renfro, N.D.; Palke, A.C.; Sun, Z.; McClure, S.F. Geographic Origin Determination of Emerald. *Gems Gemol.* **2019**, *55*, 614–646. [CrossRef]

48. Rudnick, R.L.; Gao, S. 4.1—Composition of the Continental Crust. In *Treatise on Geochemistry*, 2nd ed.; Holland, H.D., Turekian, K.K., Eds.; Elsevier Science: Amsterdam, The Netherlands, 2014; pp. 1–51, ISBN 978-0-08-098300-4.
49. Beny, J.M.; Piriou, B. Vibrational Spectra of Single-Crystal Topaz. *Phys. Chem. Miner.* **1987**, *15*, 148–159. [CrossRef]
50. Precisvalle, N.; Martucci, A.; Gigli, L.; Plaisier, J.R.; Hansen, T.C.; Nobre, A.G.; Bonadiman, C. F/OH Ratio in a Rare Fluorine-Poor Blue Topaz from Padre Paraíso (Minas Gerais, Brazil) to Unravel Topaz's Ambient of Formation. *Sci. Rep.* **2021**, *11*, 2666. [CrossRef]
51. Skvortsova, V.; Mironova-Ulmane, N.; Trinkler, L.; Chikvaidze, G. Optical Properties of Natural Topaz. *IOP Conf. Ser. Mater. Sci. Eng.* **2013**, *49*, 012051. [CrossRef]
52. Setkova, T.V.; Balitsky, V.S.; Spivak, A.V.; Kuzmin, A.V.; Borovikova, E.Y.; Kvas, P.S.; Balitskaya, L.V.; Nekrasov, A.N.; Zakharchenko, E.S.; Pushcharovsky, D.Y. Crystal Growth, Composition, Structure, and Raman Spectroscopy of Novel Ga,Ge-Rich Topaz. *J. Cryst. Growth* **2024**, *637–638*, 127723. [CrossRef]
53. Wise, M.A. Topaz: A Mineralogical Review. *Rocks Miner.* **1995**, *70*, 16–25. [CrossRef]
54. Menzies, M.A. The Mineralogy, Geology and Occurrence of Topaz. *Mineral. Rec.* **1995**, *26*, 5.
55. Gauzzi, T.; Graça, L.M. A Cathodoluminescence-Assisted LA-ICP-MS Study of Topaz from Different Geological Settings. *Braz. J. Geol.* **2018**, *48*, 161–176. [CrossRef]
56. Agangi, A.; Kamenetsky, V.S.; Hofmann, A.; Przybyłowicz, W.; Vladykin, N.V. Crystallisation of Magmatic Topaz and Implications for Nb–Ta–W Mineralisation in F-Rich Silicic Melts—The Ary-Bulak Ongonite Massif. *Lithos* **2014**, *202–203*, 317–330. [CrossRef]
57. Dezi, W.; Changshi, L.; Weizhou, S.; Maozhong, M.; Hongfei, L. Geochemical Characteristics and Genesis of Topaz-Bearing Porphyries in Yangbin Area of Taishun County, Zhejiang Province. *Chin. J. Geochem.* **1995**, *14*, 13–25. [CrossRef]
58. Leroy, J.L.; Rodriguez-Rios, R.; Dewonck, S. The Topaz-Bearing Rhyolites from the San Luis Potosi Area (Mexico): Characteristics of the Lava and Growth Conditions of Topaz. *Bull. Société Géologique Fr.* **2002**, *173*, 579–588. [CrossRef]
59. Wasim, M.; Zafar, W.A.; Tufail, M.; Arif, M.; Daud, M.; Ahmad, A. Elemental Analysis of Topaz from Northern Areas of Pakistan and Assessment of Induced Radioactivity Level after Neutron Irradiation for Color Induction. *J. Radioanal. Nucl. Chem.* **2011**, *287*, 821–826. [CrossRef]
60. Wu, C.; Liu, S.; Gu, L.; Zhang, Z.; Lei, R. Formation Mechanism of the Lanthanide Tetrad Effect for a Topaz- and Amazonite-Bearing Leucogranite Pluton in Eastern Xinjiang, NW China. *J. Asian Earth Sci.* **2011**, *42*, 903–916. [CrossRef]
61. Broughton, P.L. Precious Topaz Deposits of the Llano Uplift Area, Central Texas. *Rocks Miner.* **1973**, *48*, 147–156. [CrossRef]
62. Christiansen, E.H.; Bikun, J.V.; Sheridan, M.F.; Burt, D.M. Geochemical Evolution of Topaz Rhyolites from the Thomas Range and Spor Mountain, Utah. *Am. Mineral.* **1984**, *69*, 223–236.
63. Gauzzi, T.; Graça, L.; Lagoeiro, L.; Mendes, I.; Queiroga, G. The Fingerprint of Imperial Topaz from Ouro Preto Region (Minas Gerais State, Brazil) Based on Cathodoluminescence Properties and Chemical Composition. *Mineral. Mag.* **2018**, *82*, 943–960. [CrossRef]
64. Bassoo, R.; Eames, D.; Hardman, M.F.; Befus, K.; Sun, Z. Topaz from Mason County, Texas. *Gems Gemol.* **2023**, *59*, 414–431. [CrossRef]
65. Breiter, K.; Gardenová, N.; Vaculovič, T.; Kanický, V. Topaz as an Important Host for Ge in Granites and Greisens. *Mineral. Mag.* **2013**, *77*, 403–417. [CrossRef]
66. Ponce, B.F.; Pingitore, N.E.; Hoffer, J.M.; Anthony, E.Y.; Woronow, A. Discrimination of Topaz Rhyolites by Major-Element Composition: A Statistical Routine for Geochemical Exploration. *J. Geochem. Explor.* **1993**, *49*, 269–285. [CrossRef]
67. Soufi, M. Origin and Physical-Chemical Control of Topaz Crystallization in Felsic Igneous Rocks: Contrasted Effect of Temperature on Its OH–F Substitution. *Earth-Sci. Rev.* **2021**, *213*, 103467. [CrossRef]
68. Zeug, M.; Nasdala, L.; Chanmuang, C.; Hauzenberger, C. Gem Topaz from the Schneckenstein Crag, Saxony, Germany: Mineralogical Characterization and Luminescence. *Gems Gemol.* **2022**, *58*, 2–17. [CrossRef]
69. Hawthorne, F.C. Some Systematics of the Garnet Structure. *J. Solid State Chem.* **1981**, *37*, 157–164. [CrossRef]
70. Diella, V.; Bocchio, R.; Marinoni, N.; Caucia, F.; Spalla, M.I.; Adamo, I.; Langone, A.; Mancini, L. Garnets from Val d'Ala Rodingites, Piedmont, Italy: An Investigation of Their Gemological, Spectroscopic and Crystal Chemical Properties. *Minerals* **2019**, *9*, 728. [CrossRef]
71. Kolesov, B.A.; Geiger, C.A. Raman Spectra of Silicate Garnets. *Phys. Chem. Miner.* **1998**, *25*, 142–151. [CrossRef]
72. Locock, A.J. An Excel Spreadsheet to Recast Analyses of Garnet into End-Member Components, and a Synopsis of the Crystal Chemistry of Natural Silicate Garnets. *Comput. Geosci.* **2008**, *34*, 1769–1780. [CrossRef]
73. Emerson, D. Garnet: The Colourful Silicate, a Speciality Mineral. *Preview* **2021**, *2021*, 64–71. [CrossRef]
74. Manson, D.V.; Stockton, C.M. Gem-Quality Grossular Garnets. *Gems Gemol.* **1982**, *18*, 204–213. [CrossRef]
75. Pohwat, P.W. Connoisseur's Choice: Grossular, Jeffrey Mine, Asbestos, Les Sources Municipalité Régional de Comté Estrie, Québec, Canada. *Rocks Miner.* **2014**, *89*, 424–436. [CrossRef]
76. Kanis, J.; Redmann, M. Four Hessonite Occurrences in Orissa, India. *J. Gemmol.* **1994**, *24*, 75–83.

77. Balčiūnaitė, I.; Ignatjev, I.; Kaminskas, D.; Niaura, G.; Norkus, E. Characterization of Natural Silicate Garnets by Means of Non-Destructive Testing Methods. *Chemija* **2021**, *32*, 107–126. [CrossRef]
78. Mathavan, V.; Kalubandara, S.; Fernando, G. Occurrences of Two New Types of Gem Deposits in Okkampitiya Gem Field in Sri Lanka. *J. Gemmol.* **2000**, *27*, 65–72. [CrossRef]
79. Zwaan, P.C. Sri Lanka: The Gem Island. *Gems Gemol.* **1982**, *18*, 62–71. [CrossRef]
80. Antao, S.M. Crystal Chemistry of Six Grossular Garnet Samples from Different Well-Known Localities. *Minerals* **2021**, *11*, 767. [CrossRef]
81. Geiger, C.A.; Stahl, A.; Rossman, G.R. Raspberry-Red Grossular from Sierra de Cruces Range, Coahuila, Mexico. *Eur. J. Mineral.-Ohne Beih.* **1999**, *11*, 1109–1114. [CrossRef]
82. Spiridonov, E.; Alferova, M.; Fattykhov, T. Gem Minerals from the Saranovskoye Chromite Deposit, Western Urals. *J. Gemmol.-Lond.* **2006**, *30*, 91. [CrossRef]
83. Adamo, I.; Diella, V.; Pezzotta, F. Tsavorite and Other Grossulars from Itrafo, Madagascar. *Gems Gemol.* **2012**, *48*, 178–187. [CrossRef]
84. Farringer, G.A. Garnet. *Rocks Miner.* **1968**, *43*, 356–357. [CrossRef]
85. Mc Cauley, C. *Gem Stone Resources of South Carolina*; *Bullettin n.30*; Division of Geology, State Development Board: Columbia, SC, USA, 1964.
86. Akizuki, M. Growth Structure and Crystal Symmetry of Grossular Garnets from the Jeffrey Mine, Asbestos, Quebec, Canada. *Am. Mineral.* **1989**, *74*, 859–864.
87. Koivula, J.I.; CG, G. Fracturing in Canadian Hessonites. *J. Gemmol.* **1985**, *19*, 579–583. [CrossRef]
88. Wilson, B.S. Colored Gemstones from Canada. *Rocks Miner.* **2009**, *85*, 24–43. [CrossRef]
89. Williams, B.; Williams, C.; Yousuf, A.M.; Laurs, B.M. Hessonite from Somaliland. *J. Gemmol.* **2020**, *37*, 135–136. [CrossRef]
90. Stockton, C.M.; Manson, D.V. A Proposed New Classification for Gem-Quality Garnets. *Gems Gemol.* **1985**, *21*, 205–218. [CrossRef]
91. Bohingamuwa, W.; Gunasena, K. Sri Lankan Garnet and Garnet Beads in the Indian Ocean Maritime Trade. *J. R. Asiat. Soc. Sri. Lanka* **2018**, *63*, 103–134.
92. Bertoldi, C.; Proyer, A.; Garbe-Schönberg, D.; Behrens, H.; Dachs, E. Comprehensive Chemical Analyses of Natural Cordierites: Implications for Exchange Mechanisms. *Lithos* **2004**, *78*, 389–409. [CrossRef]
93. Liu, X.; Guo, Y. Study on the Color-Influencing Factors of Blue Iolite. *Minerals* **2022**, *12*, 1356. [CrossRef]
94. Majumdar, A.S.; Mathew, G. Raman-Infrared (IR) Spectroscopy Study of Natural Cordierites from Kalahandi, Odisha. *J. Geol. Soc. India* **2015**, *86*, 80–92. [CrossRef]
95. Kaindl, R.; Többens, D.; Haefeker, U. Quantum-Mechanical Calculations of the Raman Spectra of Mg- and Fe-Cordierite. *Am. Mineral.* **2011**, *96*, 1568–1574. [CrossRef]
96. Yan, W.; Zhou, Z.; Rao, Y.; Guo, Q. Gemological Characteristics of Blue-Violet Cordierite. *Crystals* **2024**, *14*, 637. [CrossRef]
97. Mamuse, A.; von der Heyden, B.; Blenkinsop, T. Zimbabwe's Coloured Gemstone Endowments-A Regional Geological Overview. *J. South. Afr. Inst. Min. Metall.* **2024**, *124*, 33–42. [CrossRef]
98. Hausel, W.D. A New Source of Gem-Quality Cordierite and Corundum in the Laramie Range of Southeastern Wyoming. *Rocks Miner.* **2002**, *77*, 334–339. [CrossRef]
99. Newhouse, W.H.; Hagner, A.F. *Cordierite Deposits of the Laramie Range, Albany County, Wyoming*; University of Wyoming: Laramie, WY, USA, 1949.
100. Belley, P.M. Iolite from the Thor-Odin Dome, British Columbia, Canada: Geology, Chemical Composition, Inclusions, and Cause of Chatoyancy. *Gems Gemol.* **2023**, *59*, 340–355. [CrossRef]
101. Hreus, S.; Novák, M.; Stubna, J. Iolite from the Czech Republic. *J. Gemmol.* **2022**, *38*, 12–14. [CrossRef]
102. Santosh, M.; Collins, A.S. Gemstone Mineralization in the Palghat-Cauvery Shear Zone System (Karur-Kangayam Belt), Southern India. *Gondwana Res.* **2003**, *6*, 911–918. [CrossRef]
103. Das, S.K.; Mohanty, J.K. Characteristics of Cordierite (Iolite) of Bandarguha-Orabahala Area, Kalahandi District, Odisha, India. *J. Geol. Geophys.* **2017**, *6*, 1–8. [CrossRef]
104. Zwaan, P. Enstatite, Cordierite, Kornuperine, and Scapolite with Unusual Properties from Embilipitiya, Sri Lanka. *Gems Gemol.* **1996**, *32*, 262–269. [CrossRef]
105. Malcherek, T.; Domeneghetti, M.C.; Tazzoli, V.; Ottolini, L.; McCammon, C.; Carpenter, M.A. Structural Properties of Ferromagnesian Cordierites. *Am. Mineral.* **2001**, *86*, 66–79. [CrossRef]
106. Grew, E.S.; Chernosky, J.V.; Werding, G.; Abraham, K.; Marquez, N.; Hinthorne, J.R. Chemistry of Kornerupine and Associated Minerals, a Wet Chemical, Ion Microprobe, and X-Ray Study Emphasizing Li, Be, B and F Contents. *J. Petrol.* **1990**, *31*, 1025–1070. [CrossRef]
107. Grew, E.S.; Abraham, K.; Medenbach, O. Ti-Poor Hoegbomite in Kornerupine-Cordierite-Sillimanite Rocks from Ellammankovilpatti, Tamil Nadu, India. *Contrib. Mineral. Petrol.* **1987**, *95*, 21–31. [CrossRef]

108. Martiniello, S.; Legnaioli, S.; Lorenzetti, G.; Raneri, S. The Relic and Reliquary of St. John the Baptist in Siena (Italy) and Their Gems. *J. Cult. Herit.* **2024**, *67*, 443–451. [CrossRef]
109. Kingma, K.J.; Hemley, R.J. Raman Spectroscopic Study of Microcrystalline Silica. *Am. Mineral.* **1994**, *79*, 269–273.
110. Jiang, Y.; Guo, Y. Genesis and Influencing Factors of the Colour of Chrysoprase. *Sci. Rep.* **2021**, *11*, 9939. [CrossRef]
111. Liu, K.; Guo, Y. Comparative Study of Mineralogical Characteristics of Natural and Synthetic Amethyst and Smoky Quartz. *Crystals* **2022**, *12*, 1735. [CrossRef]
112. Henn, U.; Schultz-Güttler, R. Review of Some Current Coloured Quartz Varieties. *J. Gemmol.* **2012**, *33*, 29–43. [CrossRef]
113. Bonewitz, R.; Carruthers, M.W.; Efthim, R. *Rock and Gem*; DK Publishing: London, UK, 2005.
114. Hardcastle, F. Raman Spectroscopy of Titania (TiO_2) Nanotubular Water-Splitting Catalysts. *J. Ark. Acad. Sci.* **2011**, *65*, 43–48.
115. Historical Archive and Research Department of the Uffizi Gallery. Available online: https://www.uffizi.it/en/pages/historical-archive (accessed on 14 January 2025).
116. Götze, J.; Pan, Y.; Müller, A. Mineralogy and Mineral Chemistry of Quartz: A Review. *Mineral. Mag.* **2021**, *85*, 639–664. [CrossRef]
117. Nassau, K. The Early History of Gemstone Treatments. *Gems Gemol.* **1984**, *20*, 22–33. [CrossRef]
118. Fabel, G.W.; White, W.B.; White, E.W.; Roy, R. Structure of Lunar Glasses by Raman and Soft X-Ray Spectroscopy. *Proc. Lunar Sci. Conf.* **1972**, *3*, 939–951.
119. Alvarez, M.A.; Coy-Yll, R. Raman Spectra of Tourmaline. *Spectrochim. Acta Part A Mol. Spectrosc.* **1978**, *34*, 899–908. [CrossRef]
120. Kunicki-Goldfinger, J.; Madl, M.; Dzierzanowski, P. *Late 17th Century Glass Vessels from Eiland-Technological Approach*; Annual Report of the Institute of Nuclear Chemistry and Technology; Institute of Nuclear Chemistry and Technology: Warsaw, Poland, 2007; pp. 136–141, ISSN 1425-204X.